Chapter 1. Quantum Optics and Photonics

Academic and Research Staff

Professor Shaoul Ezekiel, Dr. Selim M. Shahriar, Dr. Byoung S. Ham, Dr. Anantharaman Kumarakrishnan, Dr. Venkataduram S. Sudarshanam, Dr. Xiao-Wei Xia

Visiting Scientists and Research Affiliates

Dr. Philip Hemmer, Dr. Mikhail D. Lukin, Dr. Susanne F. Yelin, Michelle Henrion[1]

Graduate Students

Michael Bock, Jeffrey A. Bowers, Brian C. Demsky, Niell Elvin, Jacob A. Morzinski, Richard J. Nelson, Etsuko Nomo,[2] Ying Tan, Lily Wong, Ward P. Weathers

Undergraduate Students

Beng-teck Lim, Tanya Zelevinsky

Technical and Support Staff

John D. Kierstead, Juanita Riccobono

1.1 Introduction

Project Staff

Professor Shaoul Ezekiel, Dr. Selim M. Shahriar, Dr. Byoung S. Ham, Dr. Anantharaman Kumarakrishnan, Dr. Venkataduram S. Sudarshanam, Dr. Xiao-Wei Xia, Dr. Marc Cronin-Golomb,[3] Professor Seth Lloyd, Dr. Mara G. Prentiss,[4] Professor Cardinal Warde, Professor Timothy L. Grove, Dr. Philip Hemmer, Dr. Mikhail D. Lukin, Dr. Susanne F. Yelin, Michelle Henrion, Etsuko Nomo, Jeffrey A. Bowers, Ying Tan, Jacob A. Morzinski, Richard J. Nelson, Brian C. Demsky, Lily Wong, Niell Elvin, Michael Bock, Ward P. Weathers, Beng-teck Lim, Tanya Zelevinsky, John D. Kierstead, Juanita Riccobono

We have conducted research into several areas, including non-linear optics, quantum computing, atom-optics, and optical memory. In section 1.2, we present a ring resonator using a rubidium vapor optical phase conjugator. Our goal in the near future is to use such a resonator to achieve spatially broad-band squeezing of quantum noise. In section 1.3, we present evidence of electromagnetically used transparency at temperatures above what is normally used for spectral holeburning. This moves us closer to our objective of frequency-multiplexed, ultra-high-density optical data storage at room temperature, using optically excited spin echoes. In section 1.4, we demonstrate an efficient four-wave mixing process in the same system, thus establishing the feasibility of holographic multiplexing in this optical storage system. In section 1.5, we present the details of the model we developed for creating a many-bit solid-state quantum computer in spectral-holeburning media. Experimental work is in progress for realizing such a quantum computer in diamond color-centers. In section 1.6, we show the numerically simulated results for a large angle, two dimensional atom-interferometer, which can be used for creating nano-structures, such as an uniform array of quantum dots, with features as small as 2 nm. We also report the successful operation of our rubidium magnetic trap, which is currently serving as the source of cold atoms for this interferometer. Finally, in section 1.7, we report successful storage and recall of nearly 2 gigabytes of data in a thick hologram. This represents a signficant step towards our goal of creating a terabyte holographic CD ROM. For more information, please visit our website at http://qop.mit.edu.

1 Northeast Photosciences, Inc., Nashua, New Hampshire.

2 Hitachi Corporation, Tokyo, Japan

3 Tufts University, Medford, Massachusetts.

4 Harvard University, Cambridge, Massachusetts.

1.2 A Ring Laser Using a Rubidium Phase Conjugator as an Amplifying Mirror

Sponsors

U.S. Air Force - Office of Scientific Research/
AASERT
Grant F49620-96-1-0308

U.S. Air Force Research Laboratory
Grant F30602-97-C-0136

Optical phase conjugation (OPC) is of interest for many applications[5] such as optical resonators, high-speed turbulence correction, and production of the squeezed vacuum state. Recently, we have been developing various types of phase conjugators using atomic vapor. Here, we report the demonstration of a ring laser in which a rubidium vapor cell provides the gain in addition to acting as a phase conjugate mirror (PCM).[6]

In previous work, we have demonstrated a double-Λ system in sodium vapor as an efficient optical phase conjugator.[7] This OPC used a coherent population trapping (CPT)[8] based grating that produced a conjugate at low pump intensity (1 W/cm^2) with high reflectivity (>50) and fast response time (<1 ms). The sodium double-Λ system has been used to correct high-speed turbulence, thus demonstrating the potential for using an atomic vapor as a practical nonlinear material.[9] While this conjugator performs well, it requires a large detuning (matching the hyperfine splitting in the ground state) between the pump and the probe beams, representing a serious impediment to extending this technique to other resonant media.

To eliminate this constraint, we reproduced the CPT-based conjugator using Zeeman sublevels of a single hyperfine ground state and polarized light.[10] This particular experiment used rubidium and matched the sodium system in performance. The transition frequencies and required power levels are also within the range of diode lasers for this rubidium system, potentially allowing inexpensive and practical systems in the future. While this scheme is much simpler than the one employed in sodium, it is still necessary to introduce a detuning (typically 80 MHz) between the two pump beams to provide the symmetry-breaking necessary for this process. Aside from the experimental inconvenience, this non-degeneracy renders this conjugator unsuitable for applications such as phase conjugate resonators.

Recently, we have demonstrated how this conjugator can be produced with degenerate frequencies by writing the gratings in a band of atoms moving with non-zero velocities and not compromising performance.[11] The optical transitions involved in this process are illustrated in Figure 5a. Here, F and B are the forward and backward pumps, respectively, S is the signal; and C is the conjugate. To illustrate the mechanisms at work in this OPC, consider, without loss of generality, the situation where all the beams are collinear, propagating in the direction $\pm z$. The Raman resonance condition for F and S (as well as for B and C) is satisfied for all values of v_z, the velocity of an atom in the z-direction. However, the laser intensity needed for producing the dark state coherence grows quadratically with v_z. For the low laser intensity used, only a band of atoms with a small range of $|v_z|$ contribute to the grating formation. The width of this band is directly proportional to the power-broadening-limited linewidth of the Raman resonance, which is typically about 2 MHz. For the experiment reported in Grove et al.,[10] this band is centered around $v_z = 0$. Thus, the frequency difference between the forward (F) and backward (B) pumps in the frame of the atoms is the same as in the laboratory frame. In the experiment reported here, we make F and B degenerate. In order to provide for the required non-degeneracy between F and B mentioned above, the band of atoms that participate in the conjugation process are now centered

5 See, for example, R.A. Fisher, ed., *Optical Phase Conjugation* (New York: Academic, 1983), chapters 13 and 14.

6 R.C. Lind and D.G. Steel, *Opt. Lett.* 6: 554 (1981); A. Yariv and S.K. Kwong, *Opt. Lett.* 11: 186 (1986).

7 P.R. Hemmer, D.P. Katz, J. Donoghue, M. Cronin-Golomb, M.S. Shahriar, and P. Kumar, *Opt. Lett.* 20: 982 (1995); T.T. Grove, M.S. Shahriar, P.R. Hemmer, Prem Kumar, V.K. Sudarshanam, and M. Cronin-Golomb, *Opt. Lett.* 22: 769 (1997).

8 G. Alzetta, A. Gozzini, L. Moi, and G. Orriols, *Nuovo Cimento B* 36: 5 (1976); H.R. Gray, R.M. Whitley, and C.R. Stroud, *Opt. Lett.* 3: 218 (1978).

9 V.K. Sudarshanam, M. Cronin-Golomb, P.R. Hemmer, and M.S. Shahriar, *Opt.Lett.* 22: 1141 (1997).

10 T.T. Grove, E. Rousseau, X.-W. Xia, M.S. Shahriar, and P.R. Hemmer, *Opt. Lett.* 22: 1677 (1997).

11 X. Xia, D. Hsiung, T. Grove, P.R. Hemmer, and M.S. Shahriar, submitted to *Opt. Commun.*

around a non-zero value of v_z such that the differential Doppler shift of F and B add up to the non-degeneracy in Grove et al.[10]

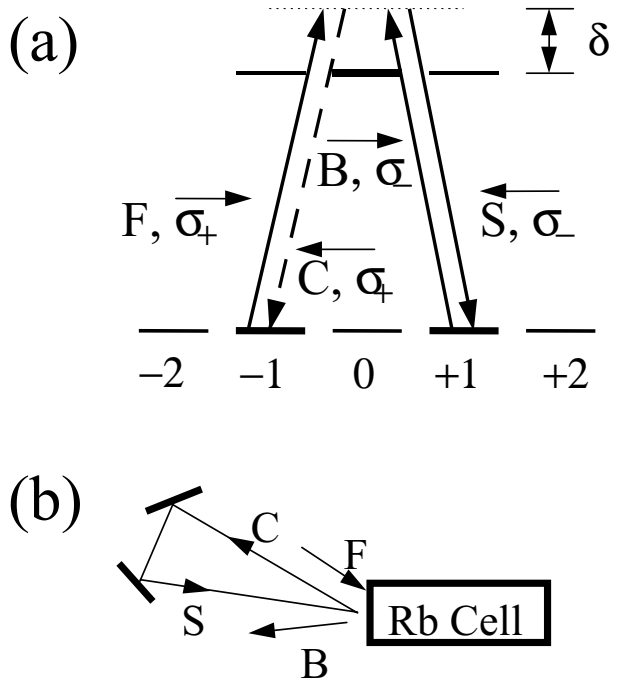

Figure 5. (a) Level diagram of the rubidium atom and the individual fields. F is the forward pump beam, B is the backward pump beam, S is the signal beam, and C is the conjugate beam. δ is determined by the pump laser detuning relative to a zero velocity atom and Δ results from the Doppler shift. (b) General method we use to create a ring cavity laser based on OPC.

Since the forward pump beam (F) and the signal beam (S) are Raman resonant, the atoms get pumped into a dark state, forming a grating in the coherence between the two ground states of the Raman transition. Here, the two ground states are Zeeman sublevels of the same hyperfine ground state. Thus, we have oppositely polarized forward pump (σ_+) and signal (σ_-) beams. The backward pump (B) diffracts off this grating and forms the conjugate beam (C). The backward beam and the conjugate beam are also Raman resonant and form a grating. The forward pump diffracts off this grating, creating an amplified signal beam. By feeding the output conjugate beam back into the system as a signal beam (using a λ/4 waveplate to correct the polarization), we create an optical resonator cavity, as shown in Figure 5b.

The experimental set up is shown in Figure 6. A single Ti:Sapphire laser produces both pump beams via beam splitters. Each of the pump beams has an FWHM of 1.0 mm, and the angle between any of the beams is less than 5 mrad. The rubidium vapor is produced inside a heat pipe oven, with Helmholtz coils to provide a magnetic field. The oven and the coils are then boxed in with μ-metal to eliminate stray magnetic fields. A ring cavity is produced when one considers the PCM created by the four-wave mixing as part of the resonator cavity. We use a 98% reflector in the cavity as an output coupler. However, we also have an effective output coupler in the amplified signal beam. In practice, we found that the signal shapes produced by these different methods yield virtually identical results.

Figure 7 shows the output power of the laser as a function of the pump beam frequency. The maximum occurs to the blue of the ^{87}Rb $5^2S_{1/2}$, F = 2 to $5^2P_{1/2}$, F = 1 transition. There is 162 mW in the forward pump and 91 mW in the backward pump. As we showed before,[12] the open-loop gain has a single Lorentzian shape, with three dips, two corresponding to the two resonances (vertical dotted lines), and one corresponding to a detuning exactly halfway between the resonances. The four peaks corresponding to the three dips would imply that we should get four peaks in the laser. The line shape observed in Figure 7 indicates that only the first two of these peaks (located around the first resonance) had a gain large enough for lasing to occur.

The output power after the 98% reflector is 0.02 mW while the amplified signal output is around 1 mW. Taking account of loss in the system due to other factors, we can estimate the internal intensities to be approximately 0.85 mW for the incident beam and 1 mW for the reflected one. This indicates a saturated gain in the PCM of around 1.2. The linear gain during the lasing build-up is of course much higher (about 40, as reported in Xia et al.[12]). Note that in a PCM laser of this form, the output power (observed as the amplified signal) is greater than the power circulating in the cavity.

12 X. Xia, D. Hsiung, M.S. Shahriar, T.T. Grove, and P.R. Hemmer, *Quantum Electronics and Laser Science Conference*, 1998.

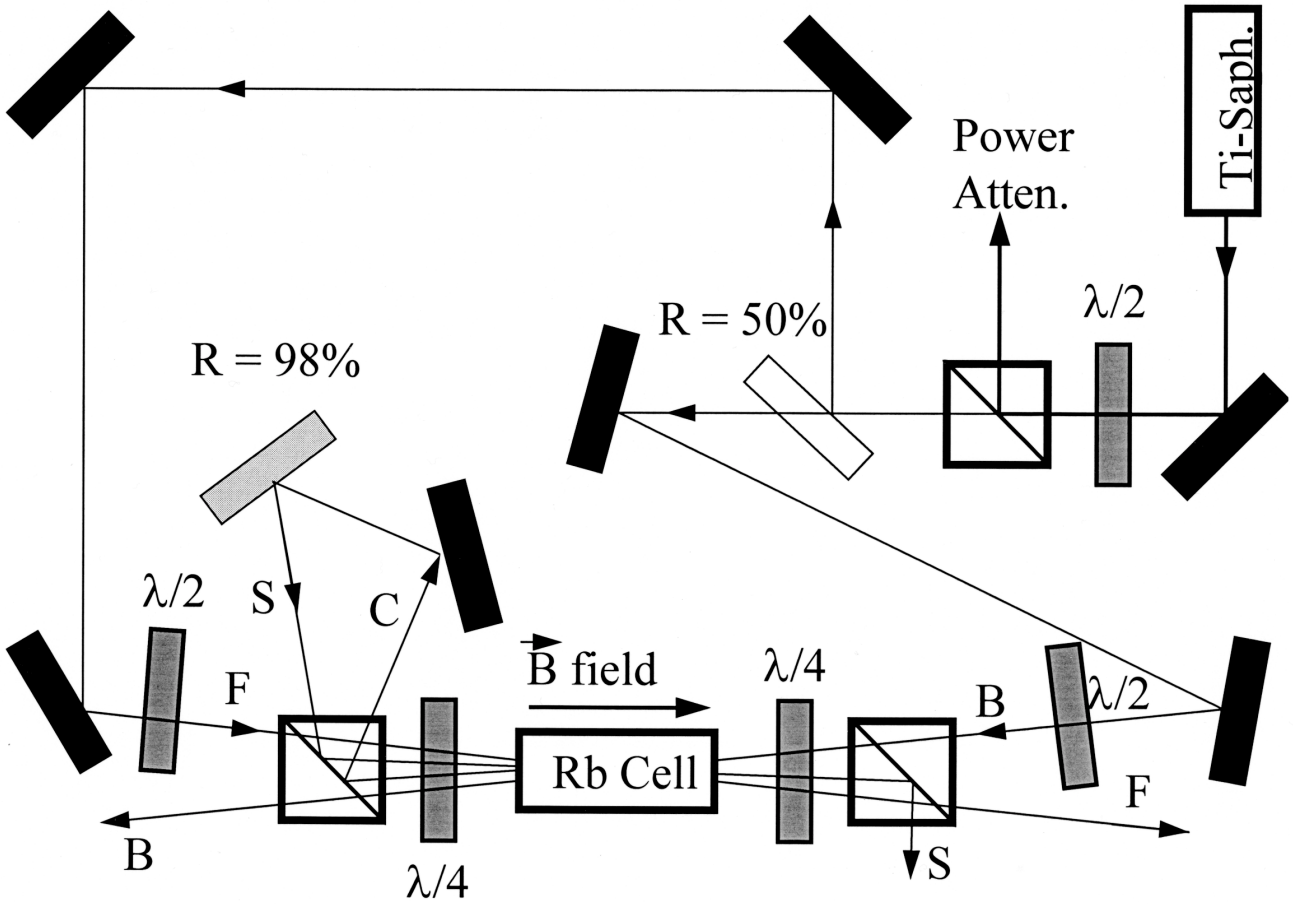

Figure 6. General experimental set up. The pump beams (F and B) are derived from a Ti:Sapphire laser and beam splitters. The resonator cavity cycles the conjugate back into the system as the signal beam.

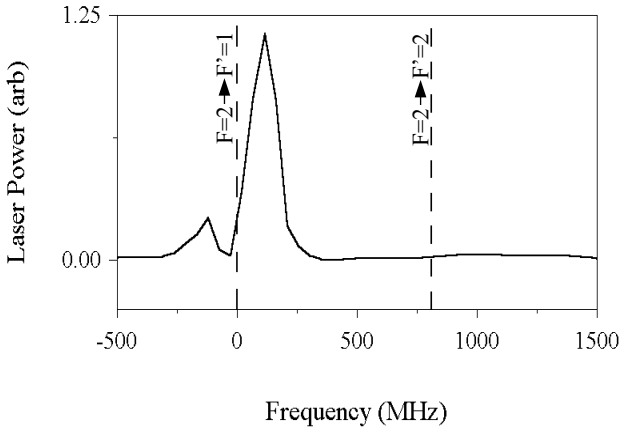

Figure 7. Pump frequency dependence of the ring laser. The largest peak occurs blue shifted to the $^{87}Rb\ 5^2S_{1/2}$, F = 2 to $5^2P_{1/2}$, F = 1 transition.

Figure 8 demonstrates the lasing dependence on the magnetic field produced by the Helmholtz coils. By using the Zeeman shift, we are able to change the effective detunings the atom sees from both the forward pump and signal beams. As the Zeeman shift is opposite for these two beams (see Figure 5), increasing the magnetic field takes the atom away from Raman resonance. As can be seen from Figure 8, the lasing width is quite narrow (<0.5 MHz FWHM). Under the open-loop conditions,[13] we have observed this linewidth to be of the order of 2 MHz. The smaller linewidth observed here is again due to the fact that the gain has to be larger than a threshold value in order for lasing to occur.

13 T.T. Grove, E. Rousseau, X.-W. Xia, M.S. Shahriar, and P.R. Hemmer, *Opt. Lett.* 22: 1677(1997); G. Alzetta, A. Gozzini, L. Moi, and G. Orriols, *Nuovo Cimento B* 36: 5 (1976).

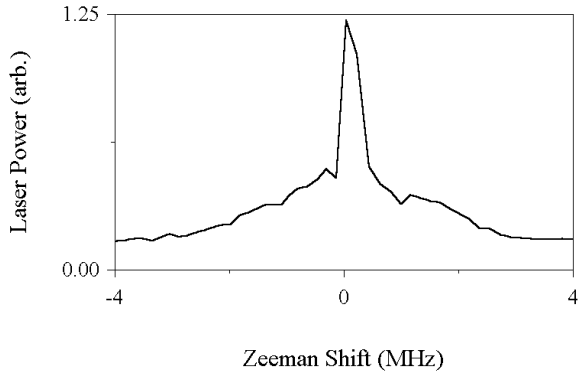

Figure 8. Lasing dependence on magnetic field. The narrow sharp peak is attributable to a Raman resonance.

Figure 9 demonstrates how the output power of the laser depends on the backward pump polarization. By inserting a λ/2 plate between the backward pump's λ/4 plate and beamsplitting cube, we can produce a backward pump with any polarization. As can be seen from the figure, the lasing is highly dependent on the polarization of the backward pump. Consistent with our model, the peak output occurs when the polarization is left circular (σ_-).

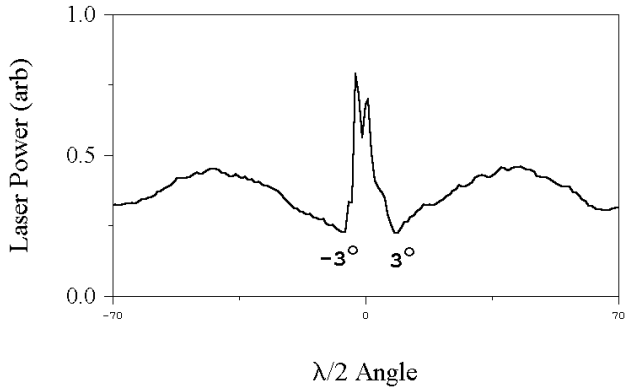

Figure 9. Lasing dependence on polarization. By inserting a λ/2 plate between the backward pump's λ/4 plate and beamsplitting cube, we can give the backward pump any polarization. The sharp peak indicates the need for a well polarized system to maintain the Λ configuration.

To summarize, we have demonstrated a ring cavity laser using the gain mechanism of a four-wave mixing process, mediated by two-photon Zeeman coherence resulting from coherent population trapping in a rubidium vapor cell. The cell has been used as an amplifying phase conjugate mirror at one corner of the ring cavity. The pump power required is low enough for a semiconductor laser. This paves the way for using the rubidium vapor cell as a conjugator for practical applications.

1.3 Observation of Electromagnetically Induced Transparency Above the Spectral-Hole-Burning Temperature Range

Sponsors

National Science Foundation
Grant ECS 94-21304
U.S. Air Force - Office of Scientific Research
Grant F49620-96-1-0395
U.S. Air Force - Rome Laboratory
Grant F30602-96-2-0100

As information technology develops, not only large-capacity storage but also high-speed information processing is important for mass data communications. Recently, spectral hole-burning materials have attracted much attention because of potential applications in mass optical data storage, fast optical switches, and computing elements such as a dynamic random access memory module. For example, the usefulness of the hole-burning materials for high-density storage[14] and high-speed optical switches[15] has been already demonstrated using photon echoes.

In the spectral hole-burning media, the storage capacity is significantly increased by wavelength multiplexing using the large ratio of inhomogeneous to homogenous width for the optical transition. This wavelength multiplexing does not suffer from Bragg degeneracy caused cross-talk,[16] which limits storage capacity in volume holographic memories. That is because adjacent spectral holes are composed of different subsets of atoms, molecules, or ions.[17] In rare earth doped solids, the storage densities are ~10^6. This large storage density, however, is only

14 H. Lin, T. Wang, and T.W. Mossberg, "Demonstration of 8-Gbit/in^2 Areal Storage Density Based on Swept-carrier Frequency-selective Optical Memory," *Opt. Lett*. 20: 1658 (1995).

15 X.A. Shen and R. Kachru, "Optical Header Recognition by Spectroholographic Filtering," *Opt. Lett*. 20: 2508 (1995).

16 D. Psaltis, D. Brady, X.-G. Gu, and S. Lin, "Holography in Artificial Neural Networks," *Nature* 343: 325 (1990); A. Chiou, "Anisotropic Cross Talk in an Optical Interconnection by using a Self-pumped Phase-conjugate Mirror at the Fourier Plane," *Opt. Lett*. 17: 1018 (1992).

available near liquid helium temperatures, because the optical homogenous width rapidly increases at higher temperatures due to phonon interactions.

Recently, a spin echo memory excited by resonant Raman pulses has demonstrated the potential to overcome the temperature restrictions in the photon echo-based memories.[18] In the resonant Raman excited spin echo memory, it was shown that the spin coherence time T_2 (reciprocal of the homogeneous width) replaces the optical T_2 for the length of the write window. Thus, under ideal conditions, the memory density is determined by the ratio of the optical inhomogeneous width to spin, rather than the optical, homogeneous width. This is especially important for higher temperature applications, because the spin homogeneous width is less temperature sensitive. For example, we demonstrated the narrower and temperature insensitive spin homogeneous width in Pr^{3+} doped Y_2SiO_5 (Pr:YSO) up to 6 K.

For the efficient Raman excited spin echoes, electromagnetically induced transparency[19] (EIT) is an essential condition. In a three-level system interacting with Raman fields, EIT is caused by destructive quantum interference, so that the optically thick medium can be transparent. Recent demonstrations of EIT[20] and resonant Raman excited spin-echoes[21] in solids, however, still required near liquid helium temperatures.

Here, we present an experimental observation of EIT in Pr:YSO at temperatures up to 15 K well beyond the spectral hole-burning temperature. We show that the probe transmission increases by a factor of exp(1.4) at 12 K.

Our system consists of 0.05 at.% Pr doped YSO in which Pr^{3+} substitutes Y^{3+}. For this work, the relevant optical transition is $^3H_4 \rightarrow {}^1D_2$, which has a frequency of ~606 nm. The inhomogeneous width of the optical transition is ~4 GHz at 1.4 K. The optical population decay time T_1 and transverse decay time T_2 are 164 μs and 111 μs, respectively at 1.4 K.[22] The ground ($^3H_4$) and excited ($^1D_2$) states have three degenerate hyperfine states, respectively. The splittings between the ground-hyperfine states are 10.2 MHz (±1/2 ↔ ±3/2), 17.3 MHz (±3/2 ↔ ±5/2), and 27.5 MHz (±1/2 ↔ ±5/2). The ground state spin decay times T_1 and T_2 are ~100 s and 500 ms,[23] respectively, at 6 K for the 10.2 MHz transition. The spin inhomogeneous width for the 27.5 MHz transition is 80 kHz at 1.6K.[24]

Figure 10 shows a schematic of the experimental setup. We use a frequency stabilized ring dye laser. The dye laser frequency jitter is about 2 MHz. For the resonant Raman transition, we excited the $^3H_4$ (±1/2) $\rightarrow {}^1D_2$ (±3/2) transition with a coupling laser and the $^3H_4$ (±5/2) $\rightarrow {}^1D_2$ (±3/2) transition with a probe laser. The coupling and probe fields are upshifted by 72.5 MHz and 100 MHz from the laser frequency, respectively. These fields are generated using acousto-optic modulators (AO) driven by frequency synthesizers (PTS 160). The probe field is fixed at resonance, while the coupling field is scanned across its resonance. The two laser beams are circularly polarized with a quarter wave plate and focused into the sample by a 25 cm focal length lens. The diameter (1/e in intensity) of the coupling laser beam is about ~50 μm in the crystal. The coupling laser intensity is varied up to a maximum of ~1.5 kW/cm^2. To produce laser

17 U.P. Wild, S.E. Bucher, and F.A. Burkhalter, "Hole Burning, Stark Effect, and Data Storage," *Appl. Opt*. 24: 1526 (1985).

18 B.S. Ham, M.S. Shahriar, M.K. Kim, and P.R. Hemmer, "Frequency-selective Time-domain Optical Data Storage by Electromagnetically Induced Transparency in a Rare-earth Doped Solid," *Opt. Lett*. 22: 1849 (1997).

19 K.J. Boller, A. Imamoglu, and S.E. Harris, "Observation of Electromagnetically Induced Transparency," *Phys. Rev. Lett*. 66: 2593 (1991).

20 Y. Zhao, C. Wu, B.S. Ham, M.K. Kim, and E. Awad, "Microwave Induced Transparency in Ruby," *Phys. Rev. Lett*. 79: 641 (1997); B.S. Ham, P.R. Hemmer, and M.S. Shahriar, "Efficient Electromagnetically Induced Transparency in a Rare-earth Doped Crystal," *Opt. Commun*. 144: 227 (1997); B.S. Ham, M.S. Shahriar, P.R. Hemmer, "Enhanced Nondegenerate Four-wave Mixing Owing to Electromagnetically Induced Transparency in a Spectral Hole-burning Crystal," *Opt. Lett*. 22: 1138 (1997).

21 B.S. Ham, M.S. Shahriar, M.K. Kim, and P.R. Hemmer, "Frequency-selective Time-domain Optical Data Storage by Electromagnetically Induced Transparency in a Rare-earth Doped Solid," *Opt. Lett.* 22: 1849 (1997); B.S. Ham, M.S. Shahriar, M.K. Kim, P.R. Hemmer, "Spin Coherence Excitation and Rephasing with Optically Shelved Atoms," *Phys. Rev. B* 58, *Rapid Comm*., forthcoming.

22 R.W. Equall, R.L. Cone, and R.M. Macfarlane, "Homogeneous Broadening and Hyperfine Structure of Optical Transitions in Pr^{3+}:Y_2SiO_5," *Phys. Rev. B* 52: 3963 (1995).

23 B.S. Ham, M.S. Shahriar, M.K. Kim, and P.R. Hemmer, "Frequency-selective Time-domain Optical Data Storage by Electromagnetically Induced Transparency in a Rare-earth Doped Solid," *Opt. Lett*. 22: 1849 (1997).

24 K. Holliday, M. Croci, E. Vauthey, and U.P. Wild, "Spectral Hole Burning and Holography in an Y_2SiO_5:Pr^{3+} Crystal," *Phys. Rev. B* 47: 14741 (1993).

pulses, we used rf switches driven by pulse generators. The pulse width is fixed at 50 μs. A Boxcar averager averages 30 samples of the probe signal. The pulse repetition rate is 50 Hz. The angle between the coupling and probe fields is about 100 mrad. The spectral hole-burning crystal of Pr:YSO is inside a cryostat, and its temperature can be varied. The size of the crystal is 3 mm × 6 mm × 1 mm. Its optical B-axis is along the 1 mm length, and laser propagation direction is almost parallel to the optical axis.

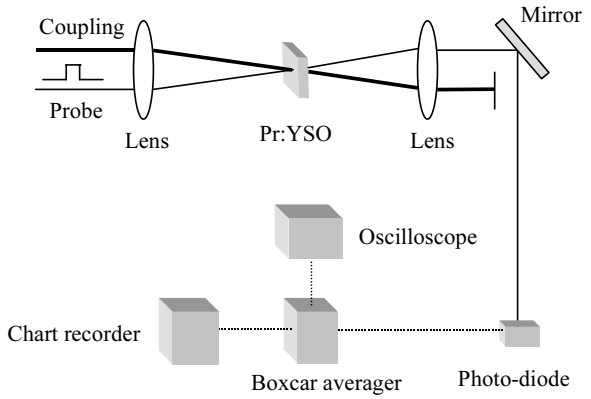

Figure 10. Schematic of the experimental setup.

Figure 11 shows the probe absorption as a function of temperature. In Figure 11, the coupling laser is blocked, and the probe intensity is adjusted not to saturate (over the temperature of the spectral hole burning). The power of the probe beam is 60 μW. Below ~8 K, the sample is nearly transparent to the probe because of spectral hole burning. The probe transmission rapidly decreases to ~10% at 10 K. The minimum transmission of the probe is 4% at 20 K. This high probe absorption continues up to ~25 K and then gradually decreases. From the data in Figure 11, the absorption coefficient α is calculated to be ~30/cm at the temperatures 12 K - 20 K.

Figure 12 shows the probe transmission versus the coupling laser detuning at 12 K. The maximum coupling laser intensity is 1.2 kW/cm^2 in the crystal. At line center (Δ = 0) of the coupling laser transition, the probe transmission is increased from 5% to 20%, a factor of exp(1.4). The FWHM of the probe transmission increase is ~2.2 MHz. This width is much narrower than the optical homogeneous width at this temperature, which is deduced to be larger than 10.2 MHz, based on the assumption that the spectral hole-burning disappears when the optical homogeneous width is larger than the ground state hyperfine splitting. This subnatural linewidth in the probe spectrum (Figure 12) is taken as evidence of EIT. Here, the efficiency of EIT is limited by available laser power. In previous work (see Zhao et al., Ham et al.[25]), more efficient EIT was seen for lower coupling laser intensity, but the temperature was much lower. This is because the EIT efficiency is inversely proportional to the homogeneous width of the optical transition, which is broader at high temperatures.

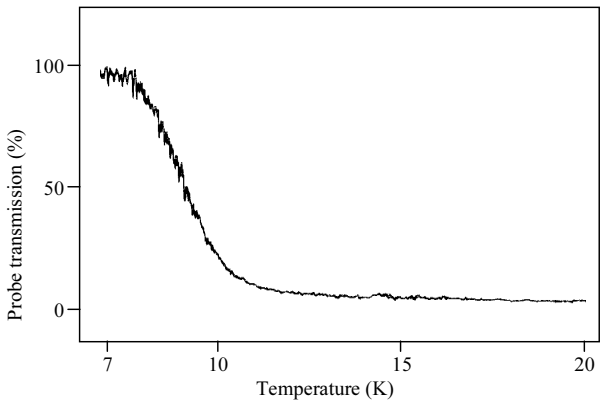

Figure 11. Probe transmission versus temperature. The probe laser power is 60 μW.

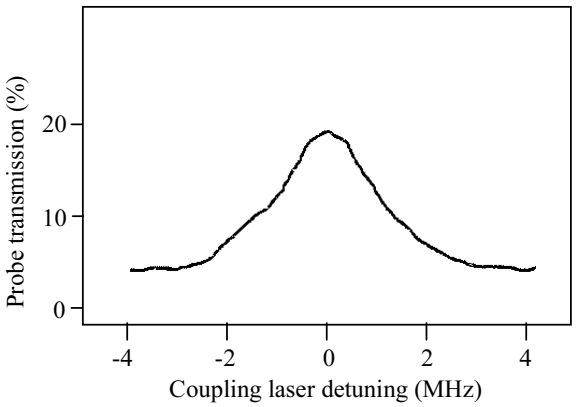

Figure 12. Probe transmission versus coupling laser detuning at 12 K.

25 Y. Zhao, C. Wu, B.S. Ham, M.K. Kim, and E. Awad, "Microwave Induced Transparency in Ruby," *Phys. Rev. Lett.* 79: 641 (1997); B.S. Ham, P.R. Hemmer, and M.S. Shahriar, "Efficient Electromagnetically Induced Transparency in a Rare-earth Doped Crystal," *Opt. Commun.* 144: 227 (1997); B.S. Ham, M.S. Shahriar, P.R. Hemmer, "Enhanced Nondegenerate Four-wave Mixing Owing to Electromagnetically Induced Transparency in a Spectral Hole-burning Crystal," *Opt. Lett.* 22: 1138 (1997).

In Figure 13, we keep the temperature at 10 K, which gives partial spectral hole burning. Initially, the probe absorption is suppressed due to EIT (see Figure 12). When the coupling laser beam is switched off (at t = 0 in Figure 13), the probe beam absorption first increases and then gradually decreases. The absorption increase at t = 0 is due to loss of EIT; coherently trapped ions begin to absorb the photons. The absorption decrease afterward is because of the spectral hole burning. The spectral hole-burning saturation time depends on the strength of the probe.

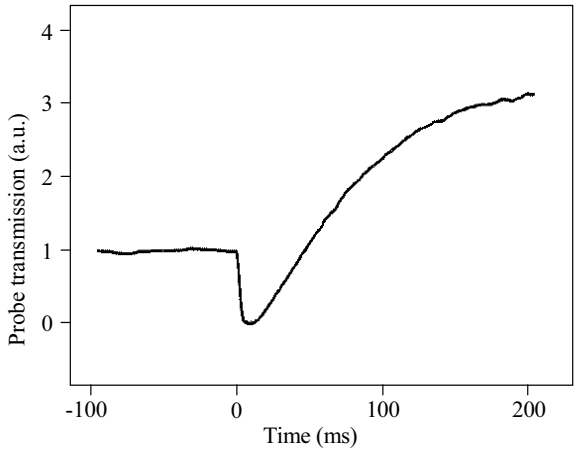

Figure 13. Probe transmission versus time. At t = 0, the coupling laser is off.

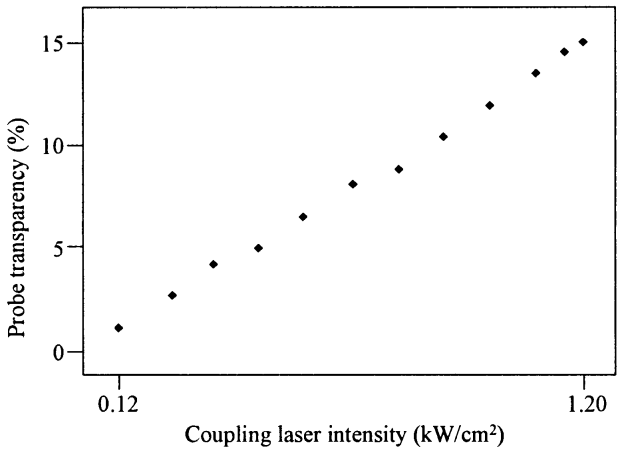

Figure 14. Probe transparency versus coupling laser intensity.

Figure 14 shows the probe transparency versus the coupling laser intensity. The temperature is fixed at 12 K. As expected, the probe transparency increases as the coupling laser intensity increases. The probe transparency increase is proportional to the square root of the coupling laser intensity. The coupling intensity axis is a log scale. For the data, the probe transparency is determined by the probe transmission change when the coupling laser is switched on.

In Figure 15, we measured the probe transparency as a function of temperature with a fixed intensity of the coupling laser. As expected, the probe transparency decreases as the temperature increases. This is because the optical homogeneous width is broadened as the temperature increases, so that the EIT efficiency decreases. Over 15 K, we could not detect the EIT effect with our maximum coupling laser intensity of ~1.2 kW/cm^2.

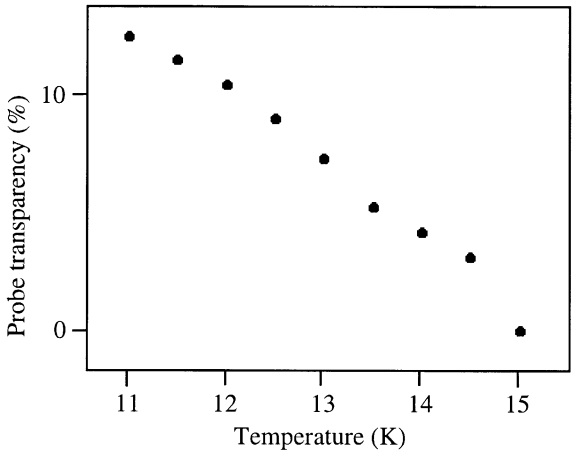

Figure 15. Probe transparency versus temperature for fixed coupling laser intensity.

To summarize, we experimentally observed EIT in an optically thick, spectral hole-burning solid of Pr:YSO at higher temperatures than needed for spectral hole-burning. This demonstration is the first step toward implementation of high-density, high-speed optical memories based on resonant Raman excited spin echoes. The Raman excited spin echo memory can achieve the higher temperature memory applications, because the spin homogeneous width is less temperature sensitive than the optical width.

1.4 Enhancement of Four-wave Mixing and Line-narrowing Using Quantum Coherence in an Optically Dense Double-Λ Solid

Sponsors

National Science Foundation
Grant ECS 94-21304
U.S. Air Force - Office of Scientific Research
Grant F49620-96-1-0395
U.S. Air Force Research Laboratory
Grant F30602-96-2-0100

Since the first proposal of enhanced nondegenerate four-wave mixing,[26] there have been several observations of the enhancement of nonlinear optical processes using two-photon coherence in gas media[27] and solids.[28] In particular, enhancement of the four-wave mixing generation in Λ-type systems is found to be large under the conditions where coherent population trapping[29] plays an essential role.[30] Without two-photon coherence, four-wave mixing efficiency is lower on resonance, because the linear susceptibility $\mathrm{Im}(\chi^{(1)})$ competes with the nonlinear susceptibility $\mathrm{Re}(\chi^{(3)})$ and suppresses the nonlinear optical processes. However, using coherent population trapping or electromagnetically induced transparency,[31] the absorption can be suppressed even at the exact resonance. Recently, nondegenerate four-wave mixing was studied using double-Λ systems in atomic[32] and molecular[33] vapors. Lu et al. demonstrated higher four-wave mixing efficiency in a double-Λ system rather than in a single-Λ system using Rb vapor.[34]

Here, we report enhanced nondegenerate four-wave mixing using a double-Λ system in an optically thick spectral-hole-burning solid, Pr^{3+} doped Y_2SiO_5 (Pr:YSO). We have observed that the probe diffraction efficiency is 2.4% in intensity (15.6% in amplitude) at 6 K, which is higher than the efficiency (< 1%) observed in a single-Λ system.[35] The observed diffraction efficiency using the double-Λ scheme in Pr:YSO is also higher than that observed in atomic[36] and molecular[37] vapors. High diffraction efficiency in a solid medium is important for potential applications such as optical memories,[38] high-resolution coherence spectroscopy,[39] lasers without population inversion,[40] and aberration correction.[41] We also report line narrowing of the four-wave mixing signal to below the inhomogeneous width of the sublevel transition. This line narrowing is due to the compression of two-photon transparency window in an

26 S.E. Harris, J.E. Field, and A. Imamoglu, *Phys. Rev. Lett*. 64: 107 (1990).

27 M. Jain, G.Y. Yin, J.E. Field, and S.E. Harris, *Opt. Lett*. 18: 998 (1993); G.Z. Zhang, K. Hakuta, and B.P. Stoicheff, *Phys. Rev. Lett*. 71: 3099 (1993); Y.-Q. Li and M. Xiao, *Opt. Lett*. 21: 1064 (1996); P.R. Hemmer, D.P. Katz, J. Donoghue, M. Cronin-Golomb, M.S. Shahriar, and P. Kumer, *Opt. Lett*. 20: 982 (1995); B. Lu, W.H. Burkett, and M. Xiao, *Opt. Lett*. 23: 804 (1998); private communications for the conversion efficiency; S. Babin, U. Hinze, E. Tiemann, and B. Wellegehausen, *Opt. Lett*. 21: 1186 (1996).

28 B.S. Ham, M.S. Shahriar, and P.R. Hemmer, *Opt. Lett*. 22: 1138 (1997).

29 H.R. Gray, R.M. Whitley, and C.R. Stroud, Jr., *Opt. Lett*. 3: 218 (1978).

30 P.R. Hemmer, D.P. Katz, J. Donoghue, M. Cronin-Golomb, M.S. Shahriar, and P. Kumer, *Opt. Lett*. 20: 982 (1995).

31 B.S. Ham, M.S. Shahriar, and P.R. Hemmer, *Opt. Lett*. 22: 1138 (1997); S.E. Harris, *Phys. Today* 50(7): 36 (1997), and references therein; B.S. Ham, P.R. Hemmer, and M.S. Shahriar, *Opt. Commun*. 144: 227 (1997); Y. Zhao, C. Wu, B.S. Ham, M.K. Kim, and E. Awad, *Phys. Rev. Lett*. 79: 641 (1997).

32 P.R. Hemmer, D.P. Katz, J. Donoghue, M. Cronin-Golomb, M.S. Shahriar, and P. Kumer, *Opt. Lett*. 20: 982 (1995); B. Lu, W.H. Burkett, and M. Xiao, *Opt. Lett*. 23: 804 (1998); private communications for the conversion efficiency.

33 S. Babin, U. Hinze, E. Tiemann, and B. Wellegehausen, *Opt. Lett*. 21: 1186 (1996).

34 B. Lu, W.H. Burkett, and M. Xiao, *Opt. Lett*. 23: 804 (1998); private communications for the conversion efficiency.

35 B.S. Ham, M.S. Shahriar, and P.R. Hemmer, *Opt. Lett*. 22: 1138 (1997); B.S. Ham, M.S. Shahriar, M.K. Kim, and P.R. Hemmer, *Opt. Lett*. 22: 1849 (1997).

36 P.R. Hemmer, D.P. Katz, J. Donoghue, M. Cronin-Golomb, M.S. Shahriar, and P. Kumer, *Opt. Lett*. 20: 982 (1995); B. Lu, W.H. Burkett, and M. Xiao, *Opt. Lett*. 23: 804 (1998); private communications for the conversion efficiency.

37 S. Babin, U. Hinze, E. Tiemann, and B. Wellegehausen, *Opt. Lett*. 21: 1186 (1996).

38 B.S. Ham, M.S. Shahriar, M.K. Kim, and P.R. Hemmer, *Opt. Lett*. 22: 1849 (1997); B.S. Ham, M.S. Shahriar, M.K. Kim, and P.R. Hemmer, *Phys. Rev. B* 58, *Rapid Comm*., forthcoming.

39 Y.S. Bai and R. Kachru, *Phys. Rev. Lett*. 67: 1859 (1991); M.D. Lukin, M. Fleischhauer, A.S. Zibrov, H.G. Robinson, V.L. Velichansky, L. Hollberg, and M.O. Scully, *Phys. Rev. Lett*. 79: 2959 (1997).

40 A.S. Zibrov, M.D. Lukin, D.E. Nikonov, L. Hollberg, M.O. Scully, V.L. Velichansky, and H.G. Robinson, *Phys. Rev. Lett*. 75: 1499 (1995), and references therein.

41 V.S. Sudarshanam, M. Cronin-Golomb, P.R. Hemmer, and M.S. Shahriar, *Opt. Lett*. 22: 1141 (1997).

optically dense medium.[42] The observed line-narrowing of the four-wave mixing signal has application to high-resolution spectroscopy.

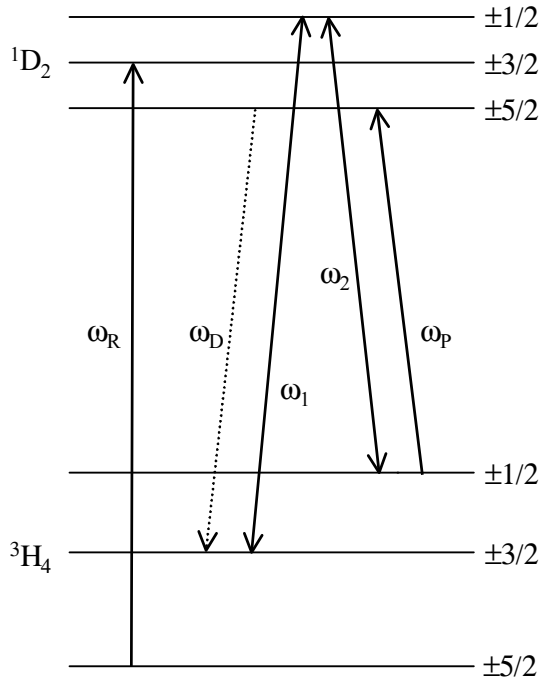

Figure 16. Energy level diagram of Pr:YSO.

Figure 16 shows an energy level diagram of Pr:YSO. Our system consists of 0.05 at.% Pr doped YSO in which Pr^{3+} substitutes Y^{3+}. For this work, the relevant optical transition is $^3H_4 \rightarrow {}^1D_2$, which has resonant frequency of 606 nm. The inhomogeneous width of the optical transition is ~4 GHz at 1.4 K.[43] The optical population decay time T_1 and transverse decay time T_2 are 164 μs and 111 μs, respectively, at 1.4 K. The ground ($^3H_4$) and excited ($^1D_2$) states have three degenerate hyperfine states, respectively. The splitting between the ground-hyperfine states is 10.2 MHz (±1/2 ↔ ±3/2), 17.3 MHz (±3/2 ↔ ±5/2), and 27.5 MHz (±1/2 ↔ ±5/2). The splitting between the excited-hyperfine states is 4.6 MHz (±1/2 ↔ ±3/2), 4.8 MHz (±3/2 ↔ ±5/2), and 9.4 MHz (±1/2 ↔ ±5/2). The ground state population decay time T_1 is ~100 s,[44] and spin transverse decay time T_2 for the 10.2 MHz transition is 500 ms at 6 K.[45] The spin inhomogeneous widths for the 10.2 MHz transition is 30 kHz at 1.6 K.[46]

The laser fields of ω_1 and ω_2 in Figure 16 act as pump beams, which create two-photon ground-state coherence via coherent population trapping. The laser field ω_P acts as a probe (read) beam, which scatters off on the two-photon coherence phase gratings created by the pump beams and generates the four-wave mixing signal ω_D satisfying phase matching condition $\mathbf{k_D=k_1-k_2+k_P}$. The repump field ω_R is used to provide spectral selectivity in the otherwise inhomogeneously broadened system (~4 GHz inhomogeneous width). The amount of spectral selectivity provided by the repump depends on the laser jitter.

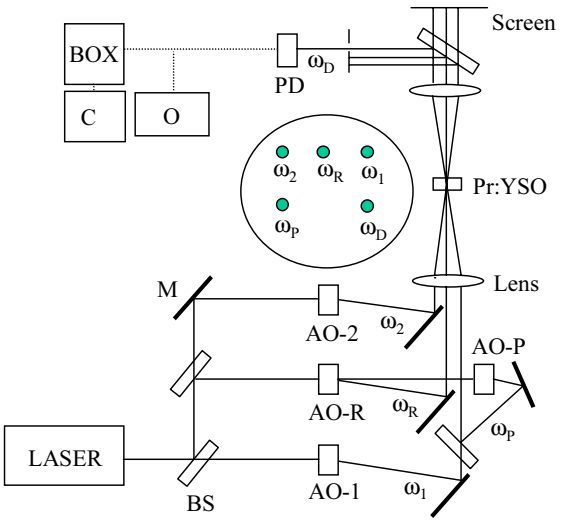

Figure 17. Schematic of the experimental setup. AO, acousto-optic modulator; BOX, box-car integrator; BS, beam splitter; C, chart recorder; M, mirror; PD, photodiode; O, oscilloscope. Inset: laser beams on screen.

Figure 17 shows a schematic of the experimental setup for the observation of nondegenerate four-wave mixing in Pr:YSO. We use a cw frequency stabilized ring dye laser pumped by a Ar-ion laser. The dye laser frequency jitter is about 2 MHz. We used acousto-optic modulators driven by frequency synthesizers (PTS 160) to make four different coherent

42 M.D. Lukin, M. Fleischhauer, A.S. Zibrov, H.G. Robinson, V.L. Velichansky, L. Hollberg, and M.O. Scully, *Phys. Rev. Lett.* 79: 2959 (1997).

43 R.W. Equall, R.L. Cone, and R.M. Macfarlane, *Phys. Rev. B* 52: 3963 (1995).

44 K. Holliday, M. Croci, E. Vauthey, and U.P. Wild, *Phys. Rev. B* 47: 14741 (1993).

45 B.S. Ham, M.S. Shahriar, M.K. Kim, and P.R. Hemmer, *Opt. Lett.* 22: 1849 (1997).

46 K. Holliday, M. Croci, E. Vauthey, and U.P. Wild, *Phys. Rev. B* 47: 14741 (1993).

laser beams as shown. For the resonant Raman transition, the pump beams ω_1 and ω_2 are downshifted by 60.0 MHz and 70.2 MHz from the laser frequency, respectively. The probe and repump field are downshifted from the dye laser output by 79.6 MHz and 47.3 MHz, respectively. All laser beams are linearly polarized and focused into the sample by a 30-cm focal length lens, so that the focused beam diameter (e^{-1} in intensity) is ~100 μm. The power of the pump lasers ω_1 and ω_2 is 12.5 mW and 9 mW, respectively. The power of the probe and repump lasers ω_P and ω_R is 18 mW and 11 mW, respectively. To produce laser pulses, we use rf switches driven by pulse generators. The pulse width of the pump and repump beams is fixed at 1 ms. The probe pulse width is 3 μs and is delayed 2 μs after the end of the pump and repump pulses. A Boxcar averager averages 30 samples of the four-wave mixing signal ω_D. The pulse repetition rate is 50 Hz. The angle between the pump and probe fields is about ~70 mrad. The spectral hole-burning crystal of Pr:YSO is inside a cryostat, and its temperature is fixed at 6 K. The size of the crystal is 3.5 mm $\times$ 4 mm $\times$ 3 mm. Its optical B-axis is along the 3 mm length, and laser propagation direction is almost parallel to the optical axis.

Figure 18 shows the efficiency of the four-wave mixing signal ω_D as a function of the detuning of the pump beam ω_2. The measured width (FWHM) is 97.0 kHz, which is two-photon power broadened. The maximum magnitude of the ω_D corresponds to a diffraction efficiency of 2.4% in intensity. The actual conversion efficiency, however, must be higher because the beams do not copropagate and the sample is optically dense. In the limit of length l longer than beam overlapping length, the four-wave mixing signal intensity (I_D) is a function of time t and distance z, which depends on the two-photon coherence (ρ_{12}) induced by two-pump fields:

$$I_D(l,t) \propto [\mathrm{Re}(\rho_{12}(z,t))]^2 \cdot I_P(0) \cdot \exp(-\alpha l)$$

where z is between 0 and l, α is an absorption coefficient, and $I_P(0)$ is the probe intensity at z = 0. In equation , the fact that four-wave mixing signal is proportional to the product of the pump intensities (until saturated) was demonstrated in atomic and molecular vapors.[47] This is because the two-photon coherence ρ_{12} is proportional to the product of pump Rabi frequencies (for weak pump beams). Using equation and the absorption coefficient $\alpha \sim 10$ cm^{-1} of the sample, we can deduce that the actual conversion efficiency of the four-wave mixing is ~11%, where we have replaced the crystal length l by effective length l′ = 1.5 mm based on 100 μm beam diameter and 70 mrad angle of intersection.

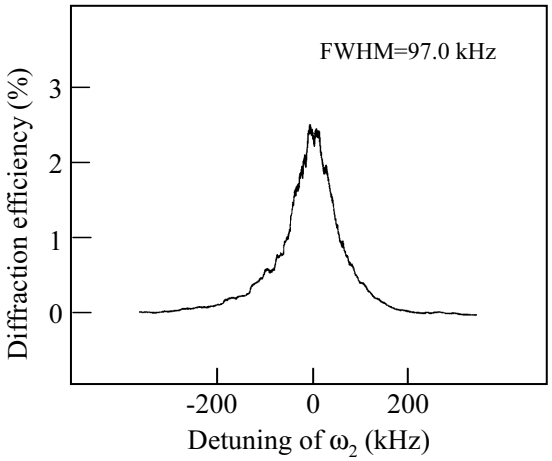

Figure 18. Four-wave mixing signal efficiency at 6 K.

For comparison, we also used an off-resonant probe beam and observed maximum diffraction efficiency of less than 1% in intensity. This was observed when the probe beam frequency is detuned ~1 MHz from the pump beam ω_2.

47 B. Lu, W.H. Burkett, and M. Xiao, *Opt. Lett.* 23: 804 (1998); private communications for the conversion efficiency; S. Babin, U. Hinze, E. Tiemann, and B. Wellegehausen, *Opt. Lett.* 21: 1186 (1996).

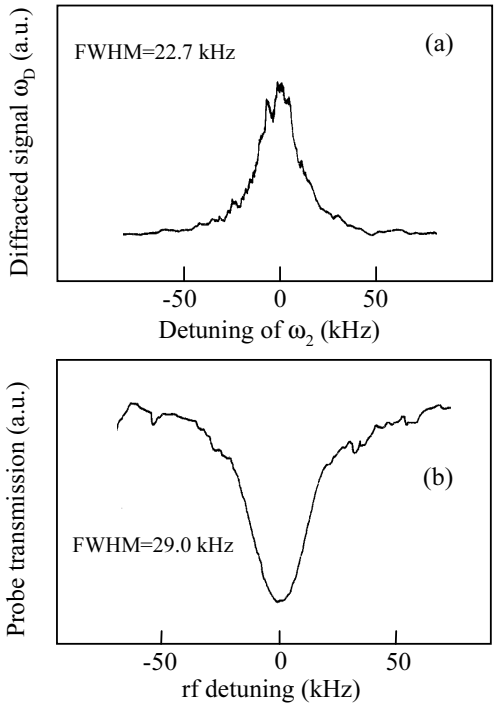

Figure 19. Line narrowing of the four-wave mixing signal.

To measure the minimum width of the two-photon coherence, we reduced the pump powers by factors of 100 and 10 for ω_1 and ω_2, respectively. Figure 19 shows the resulting diffracted signal ω_D versus the detuning of the pump beam ω_2. Here, the pump pulses are lengthened to 5ms to increase the total pulse areas to compensate lower pump intensities. We also reduced the probe power by a factor of 2. The observed width (FWHM) of the four-wave mixing signal ω_D in Figure 19 is 22.7 kHz, which is narrower by a factor of 1.3 than the inhomogeneous width (30 kHz) of the 10.2 MHz transition. This line-narrowing is attributed to the compression of the two-photon transparency window in an optically dense medium. Such line-narrowing is explained by the effects of nonlinear dispersion on parametric processes in a dense phase-coherent medium.[48] In the Lukin et al.,[42] the line-narrowing is shown to be approximately proportional to the square root of optical density, which gives a factor of 1.2 using the effective length l′ in our Pr:YSO. This is close to the observed narrowing.

To summarize, we observed enhanced nondegenerate four-wave mixing generation using a resonantly probed double-Λ scheme in an optically dense spectral hole-burning solid. The measured diffraction efficiency is 2.4% in intensity, and the conversion efficiency corrected for absorption is deduced to be ~11%. This efficient four-wave mixing has potential application to nonlinear optical processes such as optical memories, high-resolution coherence spectroscopy, lasers without population inversion, and aberration correction. We also observed line-narrowing of the four-wave mixing signal. The observed line-narrowing is due to high optical density of the medium and is useful for the high-resolution spectroscopy.

1.5 Solid-State Quantum Computing using Spectral Holeburning

Sponsors

Hertz Foundation
U.S. Air Force - Office of Scientific Research
Grant F49620-98-1-0313
U.S. Army Research Office
Grant DAAG55-98-1-0375

To perform quantum computation it is necessary to load information onto the computer, to process that information in a way that preserves quantum coherence, and to extract the results.[49] More precisely, a quantum computer that stores information on two-state systems called quantum bits or qubits must be able to address and manipulate individual qubits, to effect coherent interactions between pairs of qubits, and to read out the value of qubits. Current methods for addressing quantum bits or qubits are divided up into spatial methods, as when a laser beam is focused on an individual qubit[50] or frequency methods, as when a nuclear spin in a molecule is

48 M.D. Lukin, M. Fleischhauer, A.S. Zibrov, H.G. Robinson, V.L. Velichansky, L. Hollberg, and M.O. Scully, *Phys. Rev. Lett*. 79: 2959 (1997).

49 S. Lloyd, "A Potentially Realizable Quantum Computer," *Sci.* 261: 1569-71 (1993); D.P. DiVincenzo, "Quantum Computation," *Sci.* 270: 255-61 (1995).

50 J.I. Cirac and P. Zoller, "Quantum Computations with Cold Trapped Ions," *Phys. Rev. Lett.* 74: 4091-94 (1995); T. Pellizzari, S.A. Gardiner, J.I. Cirac, P. Zoller, "Decoherence, Continuous Observation, and Quantum Computing: a Cavity QED Model," *Phys. Rev. Lett.* 75: 3788-91 (1995); C. Monroe, D.M. Meekhof, B.E. King, W.M. Itano, and D.J. Wineland, "Demonstration of a Fundamental Quantum Logic Gate," *Phys. Rev. Lett.* 75: 4714-17 (1995).

addressed using NMR.[51] The density of qubits that can be addressed spatially is limited by the wavelength of light, and the number of qubits that can be addressed by frequency is limited by the fundamental linewidths of spins.

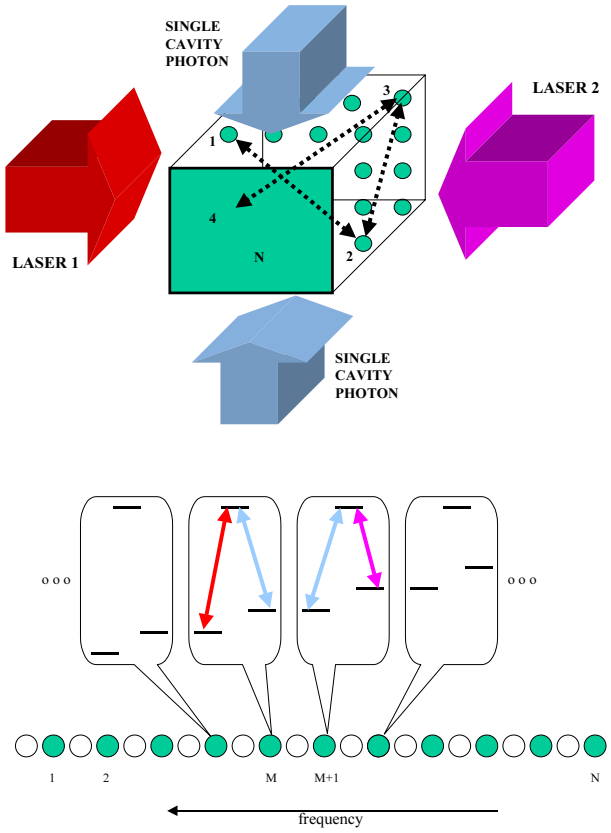

Figure 20. Schematic illustration of coupling inhomogeneously broadened atoms using spectral selectivity. The top figure shows a small volume of a crystal, selected by the intersection of the cavity mode and the control laser beams. The bottom figure shows how the atoms can be indexed in terms of their frequency response. Spectrally adjacent atoms, with a frequency difference matching the ground state splitting, can be coupled selectively by tuning the cavity and the coupling lasers. Atom M can be addressed spectrally via the red transition, atom M+1 can be addressed via the purple transition, and the two are coupled to the cavity via the blue transition.

Here, we report a method for addressing qubits using a novel method that combines spatial and spectral selectivity. The result is a design for quantum computation that provides the potential for a density of quantum information storage and processing many orders of magnitude greater than that afforded by ion traps or NMR.

The basic concept behind this method is illustrated in Figure 20. Consider a small volume (with each side being about 5λ, where λ is the wavelength of light) element of a crystal containing a set of impurity atoms, represented here by the green spheres. For current experimental tools, this is the typical volume that can be resolved spatially because of diffraction. Due to minute variations in the local environment, each of these atoms sees a unique surrounding. As a result, the resonance frequency for a given transition is different for different atoms. This effect is called inhomogeneous broadening. The number of spectrally resolvable bands, N_R, is determined by the ratio of the spectral spread to the width of the individual atomic resonance. We consider a situation where the number of impurity atoms in the selected volume equals N_R. Under this condition, achievable by controlling the level of doping, it is possible to address each atom individually.

Even when N_R is as high as 10^7, the mean interatomic distance is of the order of 10 nm, so that the atom-atom direct coupling can be ignored. As such, in order to perform quantum computing where each atom represents a qubit, it is necessary to couple the atoms to one another using external means. This can be achieved by placing the atoms in an optical cavity with a strong vacuum rabi frequency. Once two atoms are coupled by the cavity field, a wide variety of methods are potentially available for effecting quantum logic between them: essentially any form of coupling between two spectral holes, combined with the ability to perform single-hole quantum operations, allows the implementation of general purpose quantum computations.[52] Many options are available: the method that we actually choose to perform quantum logic is determined by the desire to perform two qubit operations accurately and with a minimum of decoherence. The following method is analogous to a

51 D.G. Cory, A.F. Fahmy, T.F. Havel, "Nuclear Magnetic Resonance Spectroscopy: an Experimentally Accessible Paradigm for Quantum Computing," in *PhysComp 96*, Proceedings of the Fourth Workshop on Physics and Computation, T. Toffoli, M. Biafore, J. Leao, eds., New England Complex Systems Institute, 1996, pp. 87-91; N.A. Gershenfeld and I.L. Chuang, "Bulk Spin-Resonance Quantum Computation," *Sci.* 275: 350-56 (1997).

52 D. Deutsch, A. Barenco, and A. Ekert, "Universality in Quantum Computation," *Proc. of the Royal Soc. London A* 449: 669-77 (1995); S. Lloyd, "Almost Any Quantum Logic Gate is Universal," *Phys. Rev. Lett.* 75: 346-49 (1995).

scheme proposed by Pellizzari, et al.[53] that uses adiabatic transfer to move quantum information coherently from one ion to another, then performs quantum logic by inducing single-ion Raman transitions.

Briefly, we consider a situation where each atom has a Λ-type transition, with two nondegenerate spin states coupled to a single optically-excited state. This situation is shown in Figure 20. For two atoms that are separated from each other by a frequency matching the energy difference between the low lying states, we choose a cavity frequency that excites a resonance in each atom. Via this common excitation, a cavity photon can act as a "quantum wire" over which the two atoms can exchange optical coherence. Our qubits are stored on spins, however, and so we must use optical coherence to transfer spin coherence. This can be accomplished by applying, for each of the two atoms, a laser beam coupling the remaining leg of the Λ transition. The resulting two-photon excitation acts effectively as a cavity mode exciting the spin transition, with the advantage that the excitation can be turned on or off at will by controlling the laser beams. The atoms can use the two-photon mediated quantum wire to exchange spin coherence with each other. If we tune the frequencies of the cavity as well as the laser beams by the amount corresponding to the spin transition, we can couple one of these atoms to a third one. In general, this scheme allows us to produce nearest-neighboring information exchange among a discreet set of N atoms, where N is given by the ratio of the inhomogeneous broadening to the spin transition frequency. Finally, different spots, spread in two dimensions, can be coupled by using the spatially selective version[53] of this technique, so that in principle up to 10^7N qubits (for λ in the visible range) can be all coupled to one another in a cm diameter, 10 micron thick solid using this technique.

The ability to exchange spin coherence between two atoms—a "quantum wire"—can be combined with the ability to perform coherent operations within each atom—quantum logic—to effect entanglement and to perform general purpose quantum computation. Our approach is similar to the one proposed by Pellizzari et al.[54] In order to realize this method, we require that each atom have a pair of Λ transitions that are identical to each other, as shown in Figure 21. Each atom has six low-lying spin states; for illustrative purposes it is convenient to think of these six states as resulting from multiplexing of the spin states of two constituent pseudo-particles, a spin 1 particle (A: red) and a spin ½ particle (B: blue) in each atom. In between gate operations, the logic states |0> and |1> of the qubit corresponding to every atom is represented by the spin up and down states, respectively, of B, with A in the spin horizontal state, carrying no information. These two *storage* levels are necessary in the scheme proposed here in order to avoid unwarranted excitation of populated levels in qubits adjacent to the ones involved in the gate operation. Whenever it is necessary to perform a gate operation between two neighboring gates, the information is first extracted from the storage levels. After this restoration, the logic states |0> and |1> of the qubit corresponding to atom 1 are represented by the spin up and down states, respectively, of A, with B in the spin down state, carrying no information. On the other hand, the logic states |0> and |1> of the qubit corresponding to atom 2 are represented by the spin up and down states, respectively, of B, with A in the spin down state, carrying no information.

The steps involved in entangling these two atoms are simple. First, the quantum wire is used to exchange, for example, the quantum states of the A particles. This results in the atom 2 containing all 4 bits of information: 2 in B and 2 in A, unentangled. Quantum logic operations on the two qubits now correspond to simple transitions between the spin sublevels inside atom 2. Such transitions can be used to perform controlled NOT gates and to entangle B and A. The quantum wire is now used again to exchange the states of A, resulting in the corresponding entanglement of atom 1 and atom 2. By combining inter-atom quantum wires and intra-atom quantum logic gates, it is possible in principle to build up arbitrary quantum logic circuits within the material.

53 T. Pellizzari, S.A. Gardiner, J.I. Cirac, and P. Zoller, "Decoherence, Continuous Observation, and Quantum Computing: a Cavity QED Model," *Phys. Rev. Lett.* 75: 3788-91 (1995).

54 T. Pellizzari, S.A. Gardiner, J.I. Cirac, and P. Zoller, "Decoherence, Continuous Observation, and Quantum Computing: a Cavity QED Model," *Phys. Rev. Lett.* 75: 3788-91 (1995).

The technology that can be used to implement the proposed method is spectral hole burning (SHB).[55] SHB is a proven optical technology that is currently used for high-density memories.[56] In spectral hole burning, the narrow optical line of a system such as a rare-earth ion doped in a crystal can be inhomogeneously broadened by a factor of up to 10^7. This line can be thought of as consisting of approximately 10^7 lines with the original linewidth, each shifted by some amount. Each of the shifted lines can be thought of as corresponding to a set of ions that face a similar environment within the crystalline matrix.

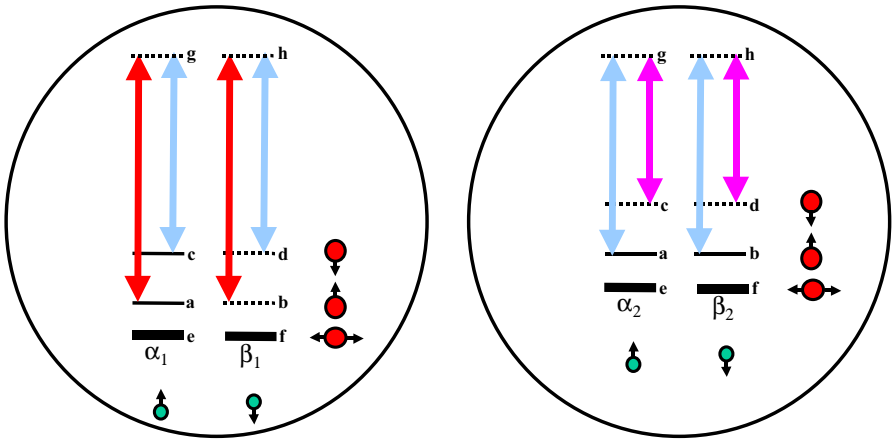

Figure 21. Relevant energy levels and transitions required of two spectrally adjacent atoms in this scheme. In each atom, the six low-lying levels can be thought of as corresponding to the spin states of two pseudo-particles: a spin 1 particle (A: red) and a spin ½ particle (B: blue). In the quiescent state, the qubit in each atoms is represented by the spin-up (0 = e) and spin-down (1 = f) states of B, with A in the spin-horizontal state, containing no information. Whenever it is necessary to perform a gate operation between two neighboring qubits, the qubit in atom 1 (α_1| e>+β_1| f>) is transferred to the spin-up and -down states of A_1, with B_1 in the spin-up state (α_1| a>+β_1| c>). This pattern is alternated in the subsequent atoms in the chain. The qubit in atom 2 (α_2| e>+β_2| f>) is transferred to the spin-up and -down states of B_1, with A_1 in the spin-up state (α_2| a>+β_2| b>). As shown by Pellizari et al.,[54] using a sequence of pulses from the red (resonant with atom 2) and orange (resonant with atom 1) lasers, the quantum states are exchanged between A_1 and A_2, via the "quantum wire" provided by the blue cavity photon, which has a common resonance with both atoms. Conceptually, this can be thought of as a two-step process. First, the orange laser transfers the state of A_1 to the cavity, producing a superposition of 0 and 1 photons (α_1| 1>+β_1| 0>). The red laser then transfers this state to A_2 (α_1| ↓>+β_1| ↑ >). All four bits of information are now in atom 2; as such, any desired gate operation (see Figure 23) can be achieved by a pulse coupling any two of the states (a,b,c,d), using a two-photon transition. A_2 is now exchanged with A_1 by using a reverse sequence of the red and orange lasers. Finally, the state of each atom is transferred to the levels e and f. These storage levels (with the e-a frequency different from the a-c frequency) are essential in this scheme in order to make sure that the populated levels of the other, quiescent neighboring qubits remain unaffected by these gate operations.

We have identified two candidate materials for implementing this technique: Pr^{3+} doped Y_2SiO_5 (Pr:YSO),[57] and nitrogen-vacancy color center in diamond (NV-diamond).[58] The relevant energy levels and their correspondence to the model are illustrated in Figure 22. Pr:YSO has the advantage that it has been well studied, both theoretically and experimentally. NV-diamond has the advantage that it has a very strong oscillator strength (of the order of the D lines of alkali atoms), so that the vacuum rabi fre-

55 R.M Macfarlane and R.M. Shelby, "Coherent Transient and Holeburning Spectroscopy of Rare Earth Ions in Solids," in *Spectroscopy of Solids Containing Rare Earth Ions*, A.A. Kaplyanskii and R.M. MacFarlane, eds. (New York: Elsevier Science Publishers B.V., 1987), pp. 51-184.

56 H. Lin, T. Wang, and T. W. Mossberg, "Demonstration of 8-Gbit/in^2 Areal Storage Density Based on Swept-carrier Frequency-selective Optical Memory," *Opt. Lett.* 20: 1658-60 (1995); X. A. Shen, E. Chiang, and R. Kachru, "Time-domain Holographic Image Storage," *Opt. Lett.* 19: 1246-48 (1994).

57 R.W. Equall, R.L. Cone, and R.M. Macfarlane, "Homogeneous Broadening and Hyperfine Structure of Optical Transitions in Pr^{3+}:Y_2SiO_5," *Phys. Rev. B* 52: 3963-69 (1995); K. Holliday, M. Croci, E. Vauthey, and U.P. Wild, "Spectral Holeburning and Holography in an Y_2SiO_5:Pr^{3+} Crystal," *Phys. Rev. B* 47: 14741-52 (1993).

58 E. VanOort, M. Glasbeek, "Optically Detected Low Field Electron Spin Echo Envelope Modulations of Fluorescent N-V Centers in Diamond," *Chem. Phys.* 143: 131 (1990); X.F. He, N.B. Manson, P.T.H. Fisk, "Paramagnetic Resonance of Photoexcited N-V Defects in Diamond. I. Level Anticrossing in the ^{3}A Ground State," *Phys. Rev. B* 47: 8809 (1993).

quency can be tens of MHz, corresponding to 10's of nanosecond time scale gate operations. Furthermore, the inhomogeneous broadening is much larger, yielding more than 10^5 qubits in a single location. By combining this with spatial coupling, as mentioned above, it should be possible to couple up to 10^{12} qubits in a cm^2, 10 micron thick crystal of NV-diamond.

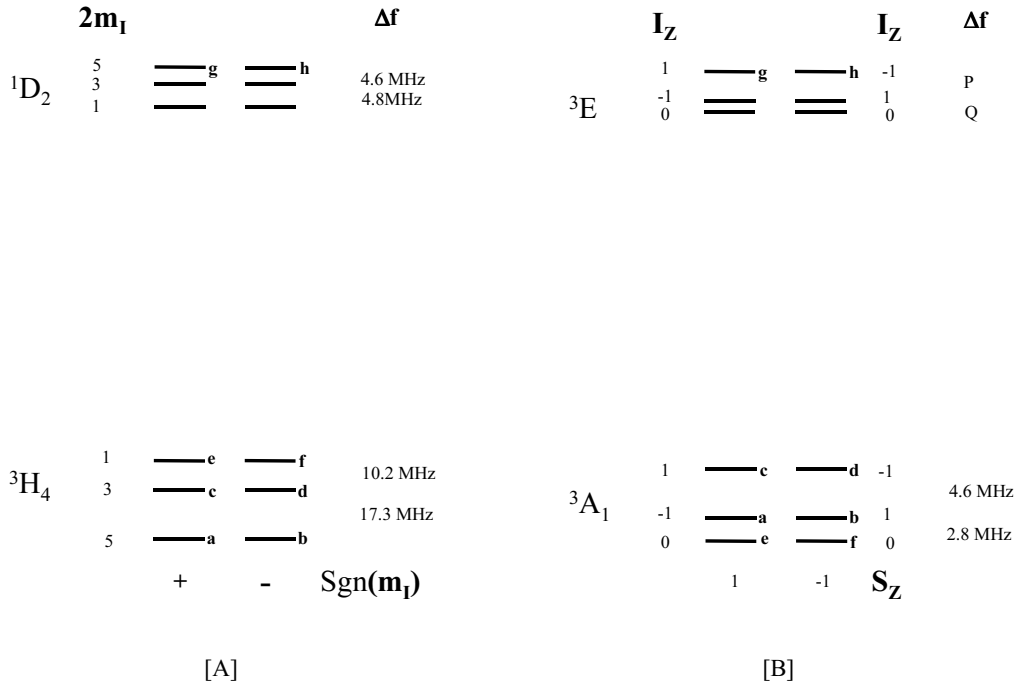

Figure 22. Relevant energy levels of two candidate solids. (a) Pr^{3+} ions in a crystal of YSO: The $^3H_4$ to $^1D_2$ transition (prohibited in free ions) is excited at 605.7 nm, with a homogeneous linewidth of 1 kHz and an inhomogeneous linewidth of 4 GHz at liquid helium temperature. In both the ground and the excited states, the energy sublevels corresponding to the different orientations of the Pr nucleus. The states corresponding to equal but opposite values of the projection quantum number (m_I) are Kramer's degenerate. The letters next to the energy levels, with reference to Figure 21, indicate the role of these levels in the present scheme for spectrally addressed gates. The additional energy levels in the excited state can facilitate the intra-atomic Raman π pulses. The 17.3 MHz frequency difference between a and c (or b and d) corresponds to the frequency interval between the gates, so that the total number of bits in a single spot is about 200. (b) N-V color centers in diamond: The $^3A_1$ to ^3E transition is excited at 637.8 nm, with a homogeneous linewidth of 5 MHz and an inhomogeneous linewidth of 1 THz at liquid helium temperature. The energy sublevels correspond to the spin orientations of the two uncoupled electrons (S) and the nucleus (I) of the substitutional nitrogen atoms. The splittings (P,Q) of the excited manifold has not yet been measured accurately but are of the order of the corresponding ground state splittings. The inter-qubit frequency spacing in this case is 4.6 MHz, corresponding to more than 10^5 qubits per spot.

As a concrete example, Figure 23 illustrates the steps used in producing an entangled state of the form $\alpha|00\rangle+\beta|11\rangle$, starting from the state $\alpha|00\rangle+\beta|10\rangle$. More general entangled states can be produced using these same steps, starting from a general state for each atom. Figure 23a shows the process of retrieving the quantum informations from the storage levels. The curved arrows here represent intra-atomic, Raman π pulses, using laser beams only. Figure 23b shows the steps involved in producing intra-atomic entanglement. First, a laser-cavity two-photon π pulse for atom 1 is used to transfer the spin coherence from A_1 (particle A in atom 1) to the quantum states of the cavity, as a superposition of 0 and 1 photons. A second laser-cavity two-photon π pulse, now for atom 2, transfers this information to A_2. Alternatively, a counterintuitive pulse sequence can be used to effect the same transfer adiabatically, which has the advantage of not suffering from spontaneous emission during the transfer. An intra-atomic Raman π pulse is now used to entangle A_2 and B_2. Finally, a reverse sequence is used to exchange A_1 and A_2, producing inter-atomic entanglement. Figure 23c shows the final step of transferring each qubit to its storage level, producing the desired state, which corresponds to a controlled-NOT operation between the two qubits.

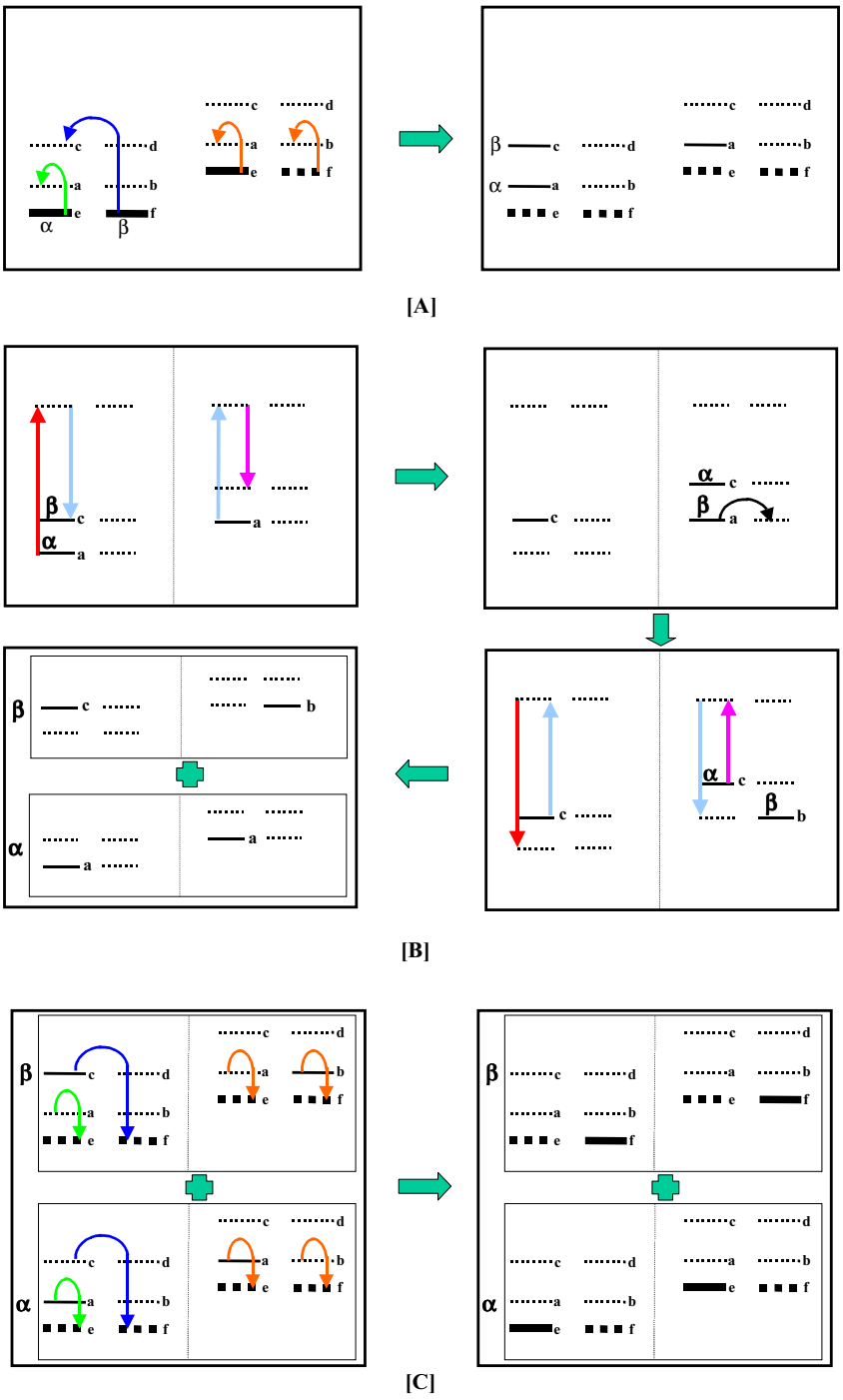

Figure 23. Illustration of the steps necessary to produce entanglement, starting from a joint state (α| 0>+β| 1>)⊗|0>. (a) The state of each qubit is retrieved from the storage levels, using off-resonance Raman π pulses, producing (α| a>+β| c>)⊗|a>; the additional levels in the excited states of both Pr:YSO and NV-diamond allow for these two-photon transitions. Either polarization selection rules or an external magnetic field can be used to provide the selectivity of the desired transition. (b) A pulse sequence of the orange and red lasers exchanges, via the common cavity photon, the states of A_1 and A_2 (see Figure 21), producing |c>⊗(α| c>+β| a>). Another off-resonance Raman π pulse is used to transfer a to b, producing |c>⊗(α| c>+β| b>); this is a controlled-NOT operation that entangles A_2 and B_2. A reverse pulse sequence of orange and red lasers exchanges back the states of A_1 and A_2, producing (α(| aa>+β| cb>), which represents an entangled state of the two atoms. (c) The state of each qubit is now returned to the storage levels, producing the final state of (α(| 00>+β| 11>), corresponding to a controlled-NOT operation between the two qubits.

During the adiabatic transfer step, there are two primary sources of decoherence: dephasing of the spin coherence and cavity losses. For example, The Pr spin coherence time T_2 is about 0.5 msec at zero magnetic field, 5 K, and a Pr concentration of 0.05 at.%. However, the spin population relaxation time T_1 is on the order of 100 sec, so that it should be possible to significantly lengthen T_2 (in principle up to the T_1 limit). Several NMR spectroscopic techniques exist for doing this and have recently been shown to be applicable to quantum computing.[59] For diamond, with a typical T_2 of 0.1 msec, it should also be possible to apply some of these techniques in order to enhance significantly the spin lifetime. Another approach is to use a diamond host free of the ^{13}C isotope, which is known to be the limiting source of spin dephasing.

Decoherence due to cavity losses can be minimized by using cavities with long photon lifetimes. Specifically, we have estimated that a concentric, hourglass cavity, with a mirror separation of 1 cm, and a Q of 2×10^5 can be used to achieve, for diamond, a vacuum rabi frequency of 17 MHz, and a cavity width of 42 kHZ.[60] The number of operations that can be performed before cavity decay is about 400. The number of operations that can be performed reliably could be extended considerably beyond this number using error-correcting codes developed specifically for this problem.[61]

To extract information from the qubits, several techniques could be used. For example, a high-Q cavity could be used to detect whether or not an atom is in a particular ground-state sublevel by applying an optical π-pulse to an appropriate transition to drive it into an excited state. Once excited, the atom can be probed by a variety of techniques such as frequency pulling of a high-Q cavity.[62] Another technique is to use a system with a cycling transition, which in turn can be used for the detection.

In summary, we have developed a model for the use of spectral holeburning materials in constructing quantum computers that have the potential to scale up to a large number of qubits. For purposes of illustration, we have explicitly outlined the steps needed to perform a quantum controlled-NOT using Pr:YSO and NV-diamond. In the case of NV-Diamond, a combination of spatial and spectral technique may enable one to couple up to 10^{12} qubits in a thin disc with a cm diameter. We have shown that it is possible in principle to load quantum information and extract results from this system and have also outlined how decoherence effects can be minimized. Finally, the use of optical beams as carriers of quantum information makes this process amenable to networking of multiple quantum computers.

1.6 Nanolithography using Atomic Interferometry

Sponsors

MIT - Undergraduate Research Opportunity Program
U.S. Air Force - Office of Scientific Research/
AASERT
Grant F49620-96-1-0308
U.S. Air Force Research Laboratory
Grant F30602-97-C-0136
U.S. Army Research Office
Grant DAG55-97-1-0103

In recent years, rapid progress has been made in the area of atom interferometry. Atomic beam gyroscopes have been demonstrated with sensitivities exceeding that of ring laser gyroscopes.[63] Such a rotation sensor may enable one to measure the general relativistic Lens-Thirring rotation in the near future. Atom interferometers have also been used to measure precisely the ratio of Planck's constant to atomic mass, acceleration due to gravity, as well as their gradients.[64] In some of these experiments, such as the gyroscope, the sensitivity is proportional to the

59 L. Viola and S. Lloyd, "Dynamical Suppression of Decoherence in Two-state Quantum Systems," *Phys. Rev. A* 58: 2733-43 (1993).

60 D.J. Heinzen, J.J. Childs, J.E. Thomas, M.S. Feld, "Enhanced and Inhibited Visible Spontaneous Emission by Atoms in a Confocal Resonator," *Phys. Rev. Lett.* 58: 1320-23 (1987); S.E. Morin, C.C. Yu, T.W. Mossberg, "Strong Atom-cavity Coupling over Large Volumes and the Observation of Subnatural Intracavity Atomic Linewidths," *Phys. Rev. Lett.* 73: 1489-92 (1994).

61 C.H. Bennett, D.P. DiVincenzo, J.A. Smolin, "Capacities of Quantum Erasure Channels," *Phys. Rev. Lett.* 78 (1997); S.J. van Enk, J.I. Cirac, and P. Zoller, "Purifying Two-bit Quantum Gates and Joint Measurements in Cavity QED," *Phys. Rev. Lett.* 79: 5178-81 (1997).

62 C.J. Hood, M.S. Chapman, T.W. Lynn, and H.J. Kimble, "Real-time Cavity QED with Single Atoms," *Phys. Rev. Lett.* 80: 4157-60 (1998).

63 T. Gustavson, P. Bouyer, and M. Kasevich, *Phys. Rev. Lett*. 78: 2046 (1997); D. Keith, C.Ekstrom, Q. Turchette, and D.E. Pritchard, *Phys. Rev. Lett.* 66: 2693 (1991).

64 M.J. Snadden et al., *Phys. Rev. Lett*. 81: 971 (1998); D.S. Weiss, B.C. Young, and S. Chu, *Phys. Rev. Lett*. 70: 2706 (1993).

area enclosed by the different paths, which in turn is determined in practice by the degree of splitting at the input port.

For the current schemes, the splitting corresponds typically to a few photon recoils. As such, there is a need for an interferometer based on a much larger splitting. Using a high-coherence-length source, such as the Bose-condensed atom laser,[65] this type of interferometer will also enable the creation of one- and two-dimensional structures with feature sizes of less than 10 nm. With chemical substitution techniques, these structures can be transferred to semiconductors or coinage metals, yielding uniform arrays of nanoquantum dots, for example.

Several schemes have been studied for realizing large angle beam splitters. The interaction of a two-level atom with a standing wave light field can produce large splitting; however, the atoms are scattered into multiple orders[66] because of the sinusoidal nature of the phase grating. The magneto-optic beam-splitter[67] and variations thereof[68] produces a triangular phase grating, which represents an improvement over the pure standing wave. Because of the subwavelength extent of the triangular shapes, however, the number of higher orders is still significant. In another scheme involving bichromatic standing waves exciting a two-level transition, the potentials remain triangular for all the dressed states, and extend over many wavelengths.[69] Both of these schemes suffer from the problem that typically the atoms are in the excited state for nearly half the time. As such, in order to minimize decoherence, the interaction time has to be small compared to the natural lifetime. This in turn limits the maximum coherent splitting to less than 20 photon recoils due to constraints imposed by high frequency modulators.

Here, we show via explicit analysis as well as numerical simulation the design of two large angle interferometers employing two-photon pulses. The first one uses the technique of adiabatic following in a dark state to produce a very large splitting atomic interferometer, as well as one-dimensional gratings with a spacing as small as 2 nm. This may lead to a nearly two orders of magnitude improvement in the sensitivity of devices such as atomic gyroscopes, which are already as good as the best laser gyroscopes. The second one uses the technique of Raman pulses to produce a *two-dimensional interferometer*, with independent choice of grating spacings in each direction, each being as small as 2 nm. This scheme may enable one to produce uniform arrays of quantum dots with dimensions of only a few nm on each side. In the near future, this process may be generalized further to produce arbitrary patterns with the same type of resolution.

The first beam splitter can achieve a splitting exceeding ±100 photon recoils and can be recombined easily to yield a high-sensitivity interferometer. For concreteness, we consider the ^{87}Rb atom, released from an evaporatively cooled magnetic trap (or a Bose condensate) and falling under gravity, as an example for this scheme. The relevant energy levels are shown in Figure 24. The atoms are assumed to be in the state $|F=1, m_f=1\rangle$ at the onset. Here, the quantization direction, **z**, is assumed to be normal to the direction of gravity, denoted as **y**.

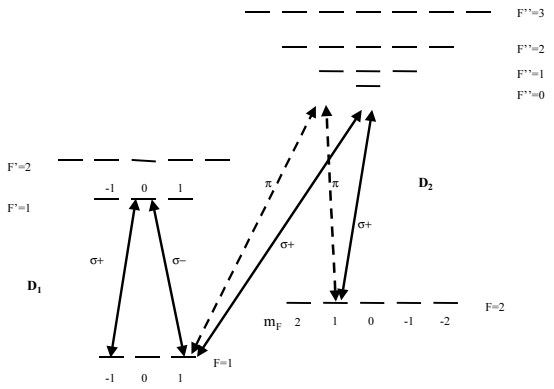

Figure 24. Schematic illustration of the relevant energy levels of ^{87}Rb atoms, considered in this article as an example. Transitions from both the D_1 and the D_2 manifolds are used. The presence of two different types of Raman transitions in the D_2 manifold, excitable by optical beams propagating in orthogonal direction, is a key element of this design.

65 M.R. Andrews et al., *Sci.* 275: 637 (1997).

66 P.L. Gould, G.A. Ruff, and D.E. Pritchard, *Phys. Rev. Lett*. 56: 827 (1986).

67 T. Pfau, C.S. Adams, and J. Mlynek, *Europhys. Lett*. 21: 439 (1993); T. Pfau et al., *Phys. Rev. Lett*. 71: 3427 (1993); U. Janicke and M. Wilkens, *Phys. Rev. A*. 50: 3265 (1994).

68 P.R. Hemmer, M.S. Shahriar, M.G. Prentiss, D.P. Katz, K. Berggren, J. Mervis, and N.P. Bigelow, *Phys. Rev. Lett*. 68: 3148 (1992); K.S. Johnson, A. Chu, T.W. Lynn, K.K. Berggren, M.S. Shahriar, and M. Prentiss, *Opt. Lett.* 20: 1310 (1995).

69 R. Grimm, J. Soding, and Yu.B. Ovchinnikov, *Opt. Lett*. 19: 658 (1994).

Using a pair of linearly polarized laser beams, co-propagating in the **x** direction, we excite the Raman transition, coupling $|F=1, m_f=1\rangle \equiv |a\rangle$ to $|F=2, m_f=1\rangle \equiv |c\rangle$, via two π-polarized transitions. The beams are detuned strongly from the excited manifold of the D_2 line, but two-photon resonant, so that the process can be thought of as a two-level transition between the two magnetic sublevels. The durations of these beams are controlled precisely, corresponding to a $\pi/2$ pulse. Ignoring the small difference between the photon recoils corresponding to the two legs of the Raman transition, we note that the center-of-mass momentum remains unchanged during this process.

The component of the atom remaining in the state $|a\rangle$ can now be deflected, in the $-\mathbf{z}$ direction, by using a set of counter-intuitively sequenced Raman pulses that couple this state to $|F=1, m_f=-1\rangle \equiv |b\rangle$, via the intermediate state of $|F'=1, m_f=0\rangle$ of the D_1 manifold.[70] Here, the optical beams are circularly polarized and propagate in the $\pm\mathbf{z}$ direction. Consider the effect of the first pair of pulses seen by the atom. The timing of the pulses, each of duration 2T, is controlled to ensure that the σ_+ polarized pulse, propagating in the $+\mathbf{z}$ direction arrives first, at time t=0. Halfway through this pulse (i.e., at t=T), the second pulse with σ_- polarization and propagating in the $-\mathbf{z}$ direction, arrives at the atom. From t=0 to t=3T, the atom evolves adiabatically, always staying in the dark state corresponding to the Raman transition: $|D\rangle \propto \{g_- |a,0\rangle - g_+|b,-2\hbar k\rangle\}$, where $g_\pm$ are the Rabi frequencies corresponding to the $\sigma_\pm$ pulses, and k is the wave number corresponding to the optical transitions. As such, at t=3T, the atom is in equal superposition of $|c,0\rangle$ and $|b,-2\hbar k\rangle$, i.e., the part in the internal state $|c\rangle$ has no momentum in the **z** direction, while the part in the internal state $|b\rangle$ has a momentum corresponding to two photon recoils in the $-\mathbf{z}$ direction. The requirement for this process to remain adiabatic is that the average Rabi frequency be much larger than the inverse of the pulse duration; this condition can be easily satisfied for pulses as short as a 10th of a nanosecond. Furthermore, note that the pulse area for this process does not have to be exact in order for the transfer to be exact.

This process is now repeated during the second pair of pulses, where the atom sees first a σ_- pulse moving in the **z** direction, followed an interval T later by a σ_+ pulse moving in the $-\mathbf{z}$ direction. After this pulse sequence, the atom ends up in equal superposition of $|c,0\rangle$ and $|a,-4\hbar k\rangle$. More generally, after 2N pairs of pulses alternated in this form, the atom is in an equal superposition of $|c,0\rangle$ and $|a,-4N\hbar k\rangle$. Figure 25 shows the results of a numerical simulation for 4N=60. Here, the curve shows the mean center of mass momentum of the $|a\rangle$ component, as a function of the total interaction time. Note that as the atoms start gaining more and more momentum, they will tend to get out of two-photon resonance.

In this simulation, this detuning has been compensated exactly by adjusting the frequency of the pulses; the same can be realized easily in an experiment as well. As such, this process may be characterized as a step-wise frequency chirped single order deflection, and, unlike most other beam-splitters/deflectors, is not bounded by the so-called Raman-Nath limit. Here, we have kept N limited to a relatively small number primarily because of computational constraints; in order to keep track of the momentum spread, the size of the density matrix scales as N^2 and the propagator for the density matrix scales as N^4. From this result, it can be inferred that the process can continue coherently for larger N, yielding momentum transfers as high as a few hundred recoils before the momentum spread would start becoming significant.

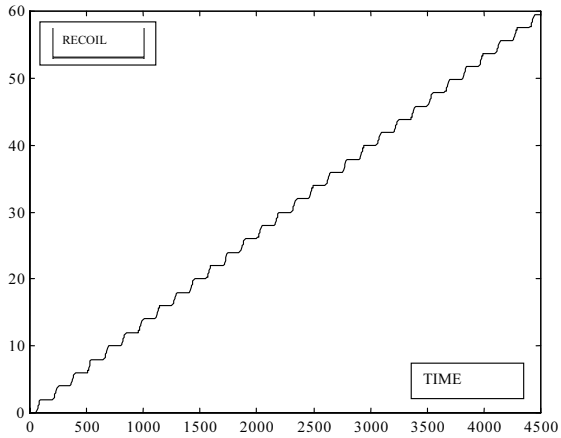

Figure 25. Result of numerical simulation, showing splitting corresponding to the absorption of 60 recoil momenta. The process, compensated for Doppler detuning, is expected to continue up to a few hundred recoils until deleterious effects of imperfect adiabatic transfers would become noticeable.

70 P. Marte, P. Zoller, and J.L. Hall, *Phys. Rev. A*. 44: R4118 (1991); M. Weitz, B.C. Young, and S. Chu, *Phys. Rev. Lett*. 73: 2563 (1994).

Let us consider a situation where 2N=50, so that at the end of the pulse sequence, the atom is in an equal superposition of |c,0> and |a,-100$\hbar$k>. We assume 3T = 150 nsec, the time required for each pair of pulses to interact with the atom, and g, the rms rabi frequency of 100 MHz, so that the adiabaticity parameter of $(2\pi g)^{-1}/T$ is about 10^{-2}, which is much less than unity, as required. The total duration for the splitting sequence is thus about 7.5 μsec. The gravitational drop during this interval is negligible compared to the size (about 1 mm) of the initial atomic cloud. Because of the velocity difference between the two components of the atomic state, the cloud will now separate spatially while falling under gravity. For ^{87}Rb atoms, the momentum difference between these two components corresponds to a transverse velocity difference of about 1 m/sec. As such, in 2 msec, for example, the atomic cloud will separate spatially, in the **z** direction, by a distance of 2 mm, while each component individually will spread much less, since the velocity spread in the initial cloud is less than a single recoil. The corresponding drop in the **y** direction, due to gravity, will be only 20 μm.

At this point, another sequence of pulses, with 2N = 100, is applied to the pulses, again along the **z** direction, with the direction of the pulses reversed, so that at the end of the pulse sequence the atom will be in an equal superposition of |c,0> and |a,+100$\hbar$k>. This process will take only about 15 μsec, so that the separation between the cloud will remain essentially unchanged. We now apply a set of linearly polarized laser beams copropagating in the **x** direction only to the |c,0> component of the atoms. Because of the large spatial separation between the clouds, this is easily possible. As before, these beams will excite off-resonant π transitions on the D_2 manifold, which will correspond to a resonant two-photon transition coupling |c,0> to |a,0>. The duration of these beams is chosen to correspond to a π pulse. Therefore, the state of the atom will now be an equal superposition of |a,0> and |a, +100$\hbar$k>, separated spatially by 2 mm.

These two clouds will now come together at the rate of about 100 cm/sec, spatially superimposing each other in about 2 msec, while dropping under gravity by about another 20 μm. The interference between these two arms will yield matter wave fringes, with a peak-to-peak spacing of about 8 nm. Using techniques that have already been well established[71] this pattern can first be deposited on a substrate coated, for example, with self-assembled monolayers of octyltrichlorosilane. The damage induced on this layer can then be transferred chemically to an underlying layer of semiconductors as well as coinage metals. This approach is obviously the preferred one for lithographic applications. Figure 26 summarizes the various steps involved in this process.

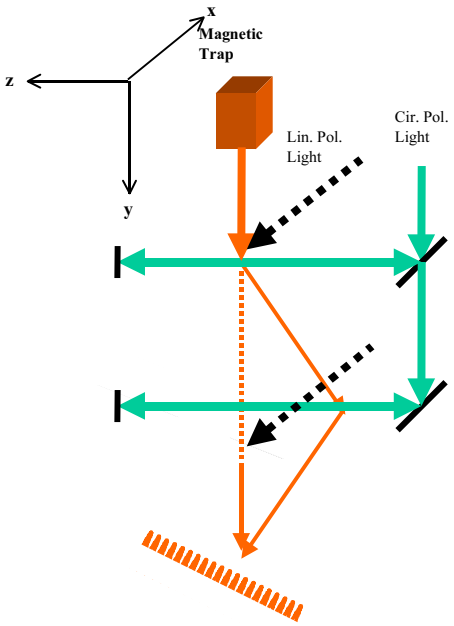

Figure 26. Schematic illustration of the three dimensional geometry employed in producing a beam splitter and recombiner via adiabatic following in the Raman dark state.

For interferometric application, another technique can be used in order to reduce the spatial period of the interference fringes, so that Ramsey techniques can be used to detect the interference. Briefly, the number of pulses during the reverse-deflection sequence would be reduced, in this case, to 2N+1=51, so that the split packets will correspond to an equal superposition of |c,0> and |b, +2$\hbar$k>. The **x** directed pulses will no longer be applied. The clouds will now converge at a much slower rate, taking 100 msec before overlapping each other, with a corresponding drop of about 5 cm due to gravity. A pair of opposite circularly polarized pulses, counterpropagating along the **z** axis, will now be applied, in order to excite a Raman transition between |c,0> and |b,+ 2$\hbar$k> states. As before, these pulses will be highly off-resonant with respect to the excited states of the D_2 manifold, with a two photon detuning denoted by

71 R. Younkin et al., *Appl. Phys. Lett*. 71: 1261 (1997).

Δ. For Δ=0, we choose a pulse duration corresponding to a $\pi/2$ pulse coupling |c,0> and |b,+ 2$\hbar$k>. This $\pi/2$ pulse will transfer all the atoms into the |b,+ 2$\hbar$k> (and not the |c,0> state, because of the sign difference introduced between the |a> and |b> states during a single step of adiabatic transfer). As Δ is scanned while the population in state |c> is observed, a Ramsey type fringe would be seen, with a frequency width corresponding to $1/\tau$, where τ is approximately equal to the time separation between the first pulse that split the atoms into the two internal states, and the last pulse that recombines them. In this case, this linewidth will be about 10 Hz, corresponding to τ of about 102 msec. Of course, any systematic phase shift between the two arms will be manifested as the corresponding shift in the fringe pattern, thus enabling detection of effects such as rotation.

For lithographic applications, it is desirable to be able to split the atomic beam in two orthogonal directions, producing four components, which would yield a two-dimensional pattern. The scheme discussed above does not render itself easily to a two-dimensional generalization. Instead a modified scheme can be used. We assume now that right after the atoms are released from the trap, they are each in state |a, p=0,q=0>≡|a,0,0>, where p corresponds to momentum in the **+z** direction, and q corresponds to momentum in the +**x** direction. We now apply, along the **z** axis, two counter-propagating, σ_+ polarized beams, exciting the transition between |a,0,0> and |c,-2$\hbar$k,0>. As before, these laser beams are assumed to be off-resonant with respect to the excited levels of the D_2 manifold, but two-photon resonant for this transition. Note that the beams have distinct frequencies, one (A) coupling |a> to an excited state, while the other (C) is of a lower frequency, coupling |c> to the same excited state.

Unlike the case of adiabatic transfers, the pulses (each of the same duration) are now timed such that they both appear at the atom at the same time, thereby leaving at the same time. First, the time duration is chosen to correspond to a $\pi/2$ transition, with A propagating in the –**z** direction, while C propagating in the +**z** direction, so that the atom ends up in an equal superposition of |a,0,0> and |c, -2$\hbar$k,0>. For concreteness, let us call this duration T′/2. The subsequent pulse pair is now assumed to be the same as before, except with a duration of T′, and the directions of A and C reversed. This will cause a π transition between |a> and |c>, producing an equal superposition of |c,+2$\hbar$k,0> and |a,-4$\hbar$k,0>. The next pulse pair is identical to this one (i.e., of suration T′), except that the directions of A and C are again reversed. The state of the atom after this pulse will now be an equal superposition of |a,+4$\hbar$k,0> and |c,-6$\hbar$k,0>. After 2P number of such alternating pulse pairs (each pair with a duration T′), the atom will be in an equal superposition of |a,+4P$\hbar$k,0> and |c,-(4P+2)$\hbar$k,0>.

Consider a case where 2P=24, so that after the sequence of pulses, the two components will differ in momentum in the **z** direction by 98 $\hbar$k and separate out with a velocity of about 100 cm/sec. Thus, as before, the cloud will split up in two parts, with a separation of 2 mm after 2 msec. For this value of 2P, the two clouds corresponds to states |a, 48$\hbar$k,0> and |c, -50$\hbar$k,0>, respectively. We now apply a set of right circularly polarized pulses, with frequencies A and C, and propagating in the opposite directions, along the **z** axis. By choosing a pair of pulses, properly sequenced in directions, and numbering 2P=48, we can now reverse the direction of each of the components, producing an equal superposition of states |a, -48$\hbar$k, 0> and |c, 46$\hbar$k, 0>.

We then apply a pair of linearly polarized beams, co-propagating along the **x** direction, causing a Raman transition between |a> and |c>.[72] The duration and spatial location of this pulse pair is chosen such that a π transition is induced between |a> and |c> only on the component of the cloud that corresponds to the state |c, 46$\hbar$k,0>. The atom is now in an equal superposition of the states |a, -48$\hbar$k,0> and |a,46$\hbar$k,0>.[73]

72 Note that because of the particular magnetic sublevels chosen as |a> and |c>, both σ_+-σ_- as well as π-π Raman transitions exist for coupling these two states. This, for example, is not the case if m_f=0 levels were chosen for both |a> and |c>, because of selection rules prohibiting Δf=0, Δm_f=0 transitions, and the constraint that $|\Delta f| \leq 1$.

73 If left alone, these components will now come together in about 2 msec, and, as before, form fringes with a peak to peak spacing of about 8 nm. Alternatively, the same technique as above can be used, by reducing the number of pulses in the deflection reversing sequence (2P=24) and skipping the x directed pulses, so that the relative momentum between the two components is only 2$\hbar$k. A $\pi/2$ pulse will then put all the atoms in the same internal state, and two-photon detuning of this pulse will yield Ramsey type interference fringes with a frequency width of about 10 Hz. For one-dimensional experiments, especially interferometry, however, the adiabatic method discussed above is preferable because of the lack of constraints on the exact pulse area.

While these two components are converging to each other in order to produce interference fringes in the **z** direction, we split each component further along the **x** axis and recombine them using a reverse sequence. Explicitly, we first apply a pair of linearly polarized beams, with frequencies A and C respectively, counter-propagating in the **x** direction. In a manner analogous to the **z** directed splitting, we first apply a $\pi/2$ pulse, interacting with both components of the split cloud, which produces an equal superposition of four states: {|a, -48$\hbar$k,0>, |c, -48$\hbar$k,-2$\hbar$k>} separated spatially in the **z** direction from {|a, 46$\hbar$k,0>, |c, 46$\hbar$k,-2$\hbar$k>}. This is followed by a series of direction-alternating π pulse pairs, numbering 2Q, producing a set of four states:

$$\{|a, -48\hbar k, 4Q\hbar k\rangle, |c, -48\hbar k, -(4Q+2)\hbar k\rangle\} \text{ and } \{|a, 46\hbar k, 4Q\hbar k\rangle, |c, 46\hbar k, -(4Q+2)\hbar k\rangle\}. \quad (1)$$

The two subclouds in curly brackets are spatially separate from each other in the **z** direction, while inside each subcloud two sub-subclouds will now separate out in the **x** direction, with a velocity of 200 cm/sec if 2Q=4P=48. Thus, after about 1 msec, the separation in the **x** direction will be about 2 mm in each subcloud. At this point, first a set of pulses totalling 2Q=96 will be applied in the **x** direction, with the timing sequences chosen so as to reverse the direction of splitting in the **x** direction. This will now produce an equal superposition of the following four states:

$$\{|a, -48\hbar k, -96\hbar k\rangle, |c, -48\hbar k, 94\hbar k\rangle\} \text{ and } \{|a, 46\hbar k, -96\hbar k\rangle, |c, 46\hbar k, 94\hbar k\rangle\}. \quad (2)$$

A **z** directed pair of copropagating, circularly polarized beams are now used to excite a π transition between |a> and |c>, but located spatially so as to affect only the |c> sub-subcloud inside each subcloud. The spatial separation of 2 mm in the **x** direction makes this selective excitation possible. After this pulse sequence, we form four pieces of clouds, converging to one another in both **x** and **z** direction, and each in the internal state |a>:

$$\{|a, -48\hbar k, -96\hbar k\rangle, |a, -48\hbar k, 94\hbar k\rangle\} \text{ and } \{|a, 46\hbar k, -96\hbar k\rangle, |a, 46\hbar k, 94\hbar k\rangle\}. \quad (3)$$

Note that the clouds are now separated in the **z** direction by 1 mm, and in the **x** direction by 2 mm. Similarly, the speed of convergence in the **z** direction (about 100 cm/sec) is half that of the convergence speed in the **x** direction. As such, all four components of the cloud will come together in another msec, forming a two-dimensional matter wave grating pattern. Figure 27 shows schematically the splitting and recombining patterns. The bottom of Figure 27 also shows the results of a numerical simulation, producing a two-dimensional grating. The spacing of these patterns are determined by the values of P and Q: the peak to peak separation in the **z** direction is given approximately (for the rubidium transition wavelength of about 800 nm) by 100/P nm, and the separation in the **x** direction is 100/Q nm. For the numbers chosen here, we thus have a grating with about 4 nm spacings in the **x** direction and 8 nm spacing in the **z** direction. Structures as small as 2 nm seems feasible given the source particles parameters considered here. The number of spots, and uniformity of height thereof, are determined largely by the coherence length of the sample. For a Bose condensed source, the coherence length is of the order of 300 μm, so that up to 10^{10} structures can be produced and deposited over an area of 300 μm diameter. In one dimension, these conclusions apply also to the adiabatic interferometer discussed above.

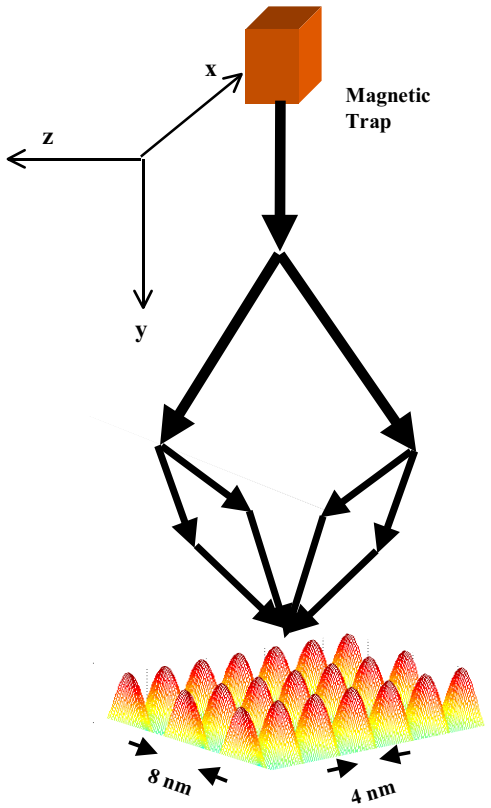

Figure 27. Basic illustration of the steps involved in producing two dimensional beam-splitting and recombining. For simplicity, the laser beams are not shown in the diagram. The two dimensional pattern at the bottom is produced via numerical simulation of the process described in the body of the text.

In summary, we have shown via explicit analysis as well as numerical simulation of the design of two large angle interferometers. The first one uses the technique of adiabatic following in a dark state to produce a very large splitting atomic interferometer, as well as one dimensional gratings as small as 2 nm spacing. This may lead to a nearly two orders of magnitude improvement in the sensitivity of devices such as atomic gyroscopes, which are already as good as the best laser gyroscopes. The second one uses the technique of Raman pulses to produce a two-dimensional interferometer, with independent choice of grating spacings in each direction, each being as small as 2 nm. This scheme may enable us to produce uniform arrays of quantum dots with dimensions only 2 nm on each side. In near future, this process may be generalized further to produce arbitrary patterns with the same type of resolution, with applications to integrated circuits.

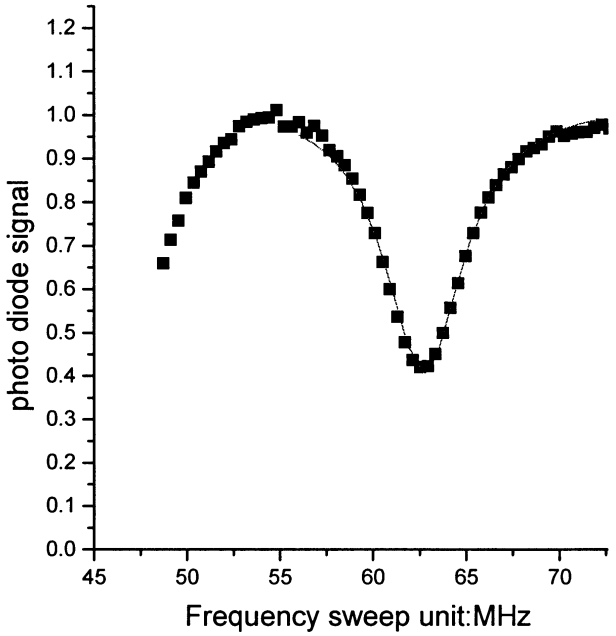

Figure 28. The absorption profile of a typical transition for the Rb atoms in our magnetic trap. Note that the linewidth is close to the natural one (5.6 MHz). Atoms from this source will be used in realizing the nanolithography experiment.

Experimental work is currently in progress in order to realize these beam splitters. Primarily, we will use atoms from a magnetic trap, before or after Bose condensation, as a source. We have recently loaded atoms from our magneto-optic trap into a magnetic trap successfully. Work is in progress to cool these atoms further, via evaporative cooling, to produce a Bose-condensed rubidium atom laser. However, even with the trap we currently have, we are ready to demonstrate the basic features of these beamsplitters. Figure 28 shows a sample scan of the atomic absorption through one of the transitions in the D_2 manifolds, using atoms held in the magnetic trap.

1.7 Long-Term Optical Data Storage in Thick Holograms

Sponsors

BMDO/Northeast Photosciences
Contract BMDO96-001

U.S. Air Force - Office of Scientific Research/
AASERT
Grant F49620-96-1-0308

The ability to store a large number of holograms in a single recording material is important for the implementation of optical neural networks, optical interconnects, and holographic computing elements. Recently, a strong effort[74] has been undertaken by several groups to develop high-volume data storage devices using holograms. The fundamental storage capacity in such a system is limited to $\sim V/\lambda^3$, where V is the volume, and λ is the wavelength of light. In practice, this limit is difficult to achieve, due primarily to cross-talks. Various techniques, including angle multiplexing, wavelength multiplexing, orthogonal phase encoding, and fractal-space multiplexing, or a combination thereof have been employed to improve the storage density, although still well below the theoretical limit.

For practical systems of wider use, it is necessary to develop holographic storage systems that will work at room temperature. In principle, a thickness of between 1 and 2 cm provides optimum storage density, due to constraints imposed by optical access requirements. Data storage using holograms of such thickness (1 cm or more) have so far only been performed in photorefractive crystals. However, photopolymeric systems generally have several distinct advantages over photorefractive systems. These

74 F.H. Mok, *Opt. Lett.* 18: 915 (1993); S. Tao, D.R. Selviah, and J.E. Midwinter, *Opt. Lett.* 18: 912 (1993); A. Chiou, *Opt. Lett.* 17: 1018 (1992); G. Rakuljic, V. Leyva, and A. Yariv, *Opt. Lett.* 17: 1471 (1992); H. Li and D. Psaltis, *Appl. Opt.* 33: 3764 (1994); H. Yu, S. Li, and D. Psaltis, *J. Opt. Sci. Am. A* 12: 1902 (1995); A. Pu and D. Psaltis, in *Proceeding of Optical Society of America Annual Meeting*, Portland, Oregon, 1995, paper MEE4; B. Kohler, S. Bernet, A. Renu, and U. Wild, *Opt. Lett.* 18: 2144 (1993).

include much lower cost, lack of constraint in shape, higher diffraction efficiency, lower refractive index (1.6, compared to 2.2 for typical photorefractives) which implies a larger field of view, simplicity of fixing, and a wide spectral bandwidth (400 to 1500 nm). As such, these material can be used to make a practical disc memory, read by compact semi-conductor lasers. For example, the lasers currently used in CD ROMS operate near 800 nm, which is near the peak of the photopolymer sensitivity, but is outside the spectral response curve of Lithium Niobate crystals.

However, to date, only thin (100 μm or less) holograms have been successfully used to demonstrate storage in photopolymeric structures.[75] This is due to a host of problems in creating thick holograms of good quality. These problems span issues such as differential shrinkage, non-uniformity of active elements through the substrate, difficulty in embedding materials into substrates, and lack of high quality optical surfaces. As a result, the full potential of holographic data storage in such media is kept limited by the useful thickness. For example, the storage achievable in a 100 μm thick hologram is theoretically two orders of magnitude smaller than what can be achieved in a 1 cm thick hologram. Even within the current limits due to optical accessing architectures, it should be possible to store as much as 150 bits/μm^2 in a 1 cm thick hologram.

We have used a material called Photopolymer with Diffusion Amplification (PDA)[76] to produce holographic substrates with an excellent surface quality and very low scattering, with almost arbitrary size and shape.[77] In particular, we have constructed a disc 5 inches in diameter, and 3 mm thick. In this substrate, we have stored and recalled nearly 2 gigabytes of optical data. With some improvements in the input-output architectures, we expect to produce a one terabyte holographic CD ROM using this substrate.

Figure 29 shows the basic optical setup used for writing the holograms. Figure 30 shows the electronic synchronization process. Figure 31 illustrates the displacement-free angular scanning geometry realized with matched galvo-scanners. Figure 32 shows a sample set of original data. Upon retrieval from the hologram, the data is quite robust, as shown in Figure 33. We expect to reach a bit error rate of 10^{-4}, by using a combination of improved optics, as well as cooled photodetectors. Finally, Figure 34 shows the relative diffraction efficiency of the 384 holographic pages written at each individual spot.

75 A. Pu and D. Psaltis, in *Proceeding of Optical Society of America Annual Meeting*, Portland, Oregon, 1995, paper MEE4; B. Kohler, S. Bernet, A. Renu, and U. Wild, *Opt. Lett.* 18: 2144 (1993).

76 A.V. Veniaminov, V.F. Goncharov, and A.P. Popov, *Optics and Spectroscopy* (USSR) 70(4): 505-08 (1991), and references therein.

77 M.S. Shahriar, L. Wong, M. Bock, B. Ham, J. Ludman, and P. Hemmer, "Ultra-high Density Optical Data Storage," *Symposium on Electro-Optics: Present and Future*, 1998, published in *Trends in Optics and Photonics*, H. Haus, ed. (Washington, DC: Optical Society of America, 1998) pp 97-104.

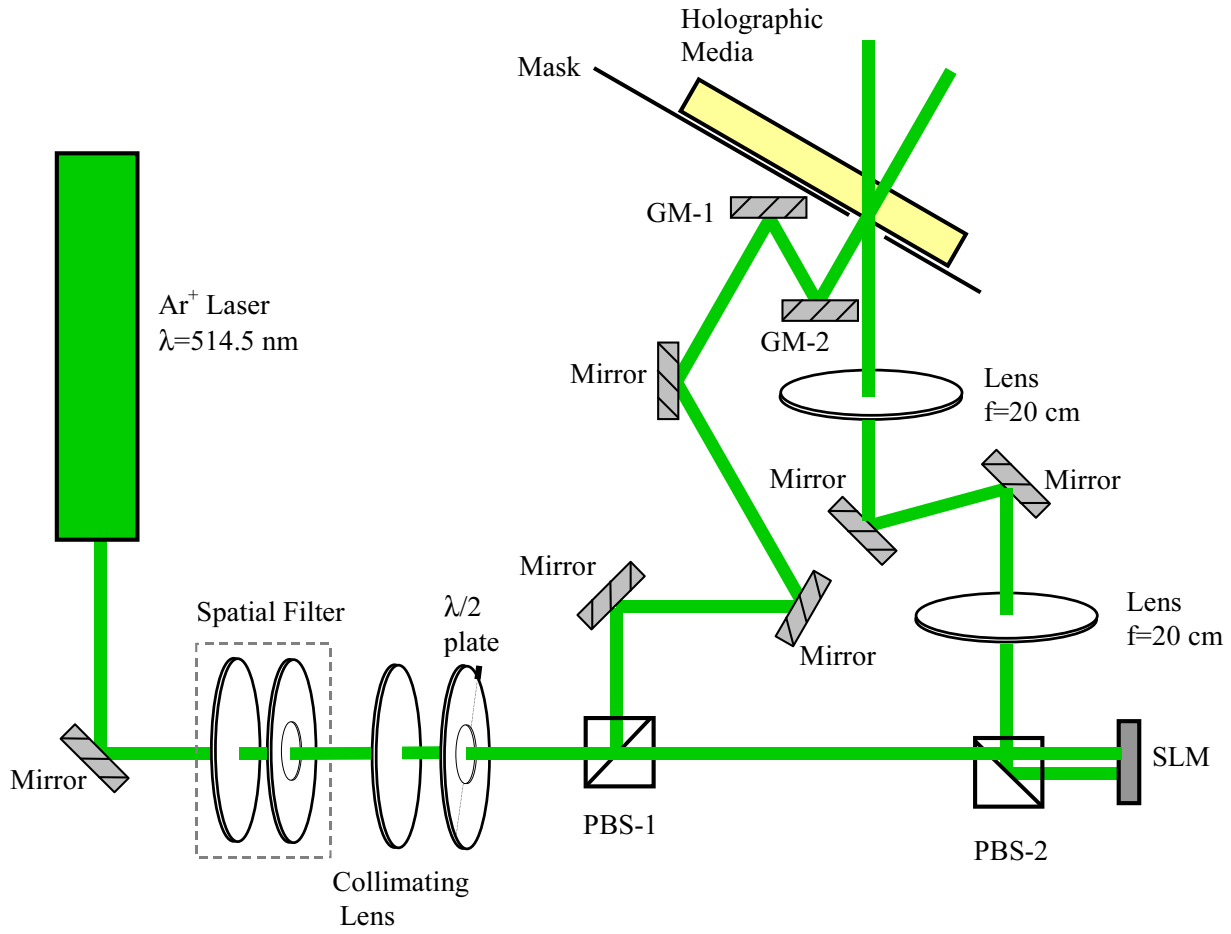

Figure 29. Optical setup for writing holograms. Light from an Ar^+ laser, λ=514.5 nm, passed through a spatial filter and was collimated. The collimated beam passed through a half-wave plate to maximize image contrast. A polarizing beam splitter, PBS-1 divided the beam into two, yielding the object and reference beams. The object beam passed through polarizing beam splitter PBS-2 to a spatial light modulator (SLM) where it received data in the form of a 256 x 256 pixel, 2-bit color depth image array. The SLM imposed the image array onto the object beam by rotating the polarization of the white pixels by 180°, while the polarization of the black pixels was unrotated. The object beam carrying the data was reflected back through the polarizing beam splitter and was imaged onto the holographic plate using 4f optics in order to minimize aberrations and to guarantee a minimum image resolution of 4 μm. This beam impinged on the holographic material at an angle of 30° from the surface normal. The separate reference and object beams travelled equal pathlengths to the unexposed holographic plate. To accomplish this, the reference beam was reflected off several mirrors before reaching the galvonometric mirrors GM-1 and GM-2. GM-1 and GM-2 were controlled electronically so that the angle at which the reference beam impinged on the material could be incremented by 1 mrad, over a range of 384 mrad. The geometrical arrangement of the galvo mirrors was chosen such that the spatial deviation of the beam on the sample was corrected for as the incident angle was varied. Angular separation of the individual holograms was 1 mrad. The angle between the object and reference beam at the central galvo mirror position was 60°. A total of 384 images were written at each spot on the holographic medium.

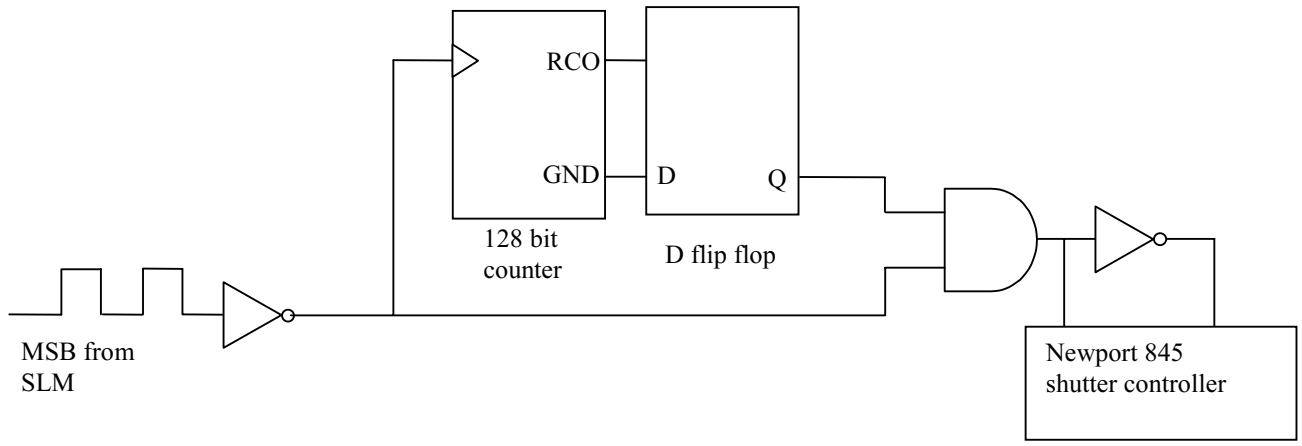

Figure 30. TTL circuit for control of the Newport 846HP shutter. The most significant bit (MSB) from the Displaytech Spatial Light Modulator was inverted and used as the clock signal. Clock cycles were counted by cascading two 16 bit counters. After 128 cycles, the ripple carry output (RCO) of the 128 bit counter triggered the D flip flop. The output from the D flip flop, which was high until triggered by the RCO, goes low such that the output at the AND gate stays low and prevents the shutter from opening.

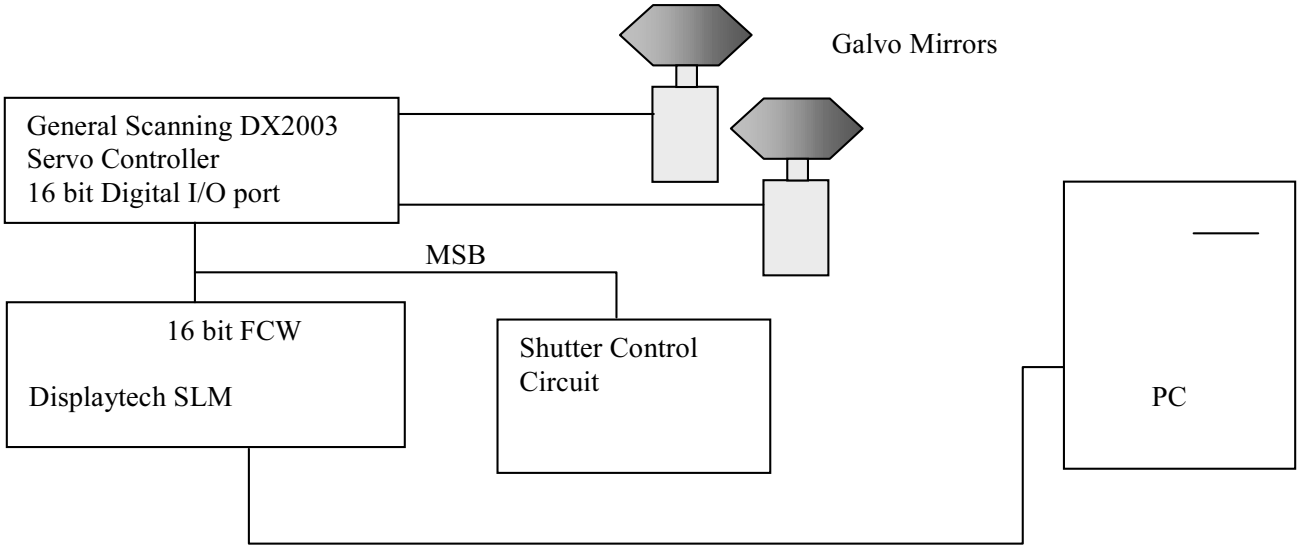

Figure 31. Schematic of electronic experimental setup. Image arrays of 256 x 256 pixels, 2-bit color depth, were downloaded to the video RAM of the spatial light modulator. The total VRAM of 1 MB limited the number of such memory pages to 128. Images and galvo mirror angle were controlled through batch files called frame rotation lists (FRLs) which specified memory page and a 16 bit frame control word (FCW), 12 bits of which were user programmable. The 12 bits were used to generate a 16 bit digital signal which was input to the general scanning controller, which controlled the angle of the galvo mirrors. In order to prevent burn in of the SLM, the inverse image was displayed immediately following normal image display. This was controlled by toggling the most significant bit (MSB) of the FCW. To prevent exposing the holographic media to the inverse image, the MSB was used to trigger a shutter.

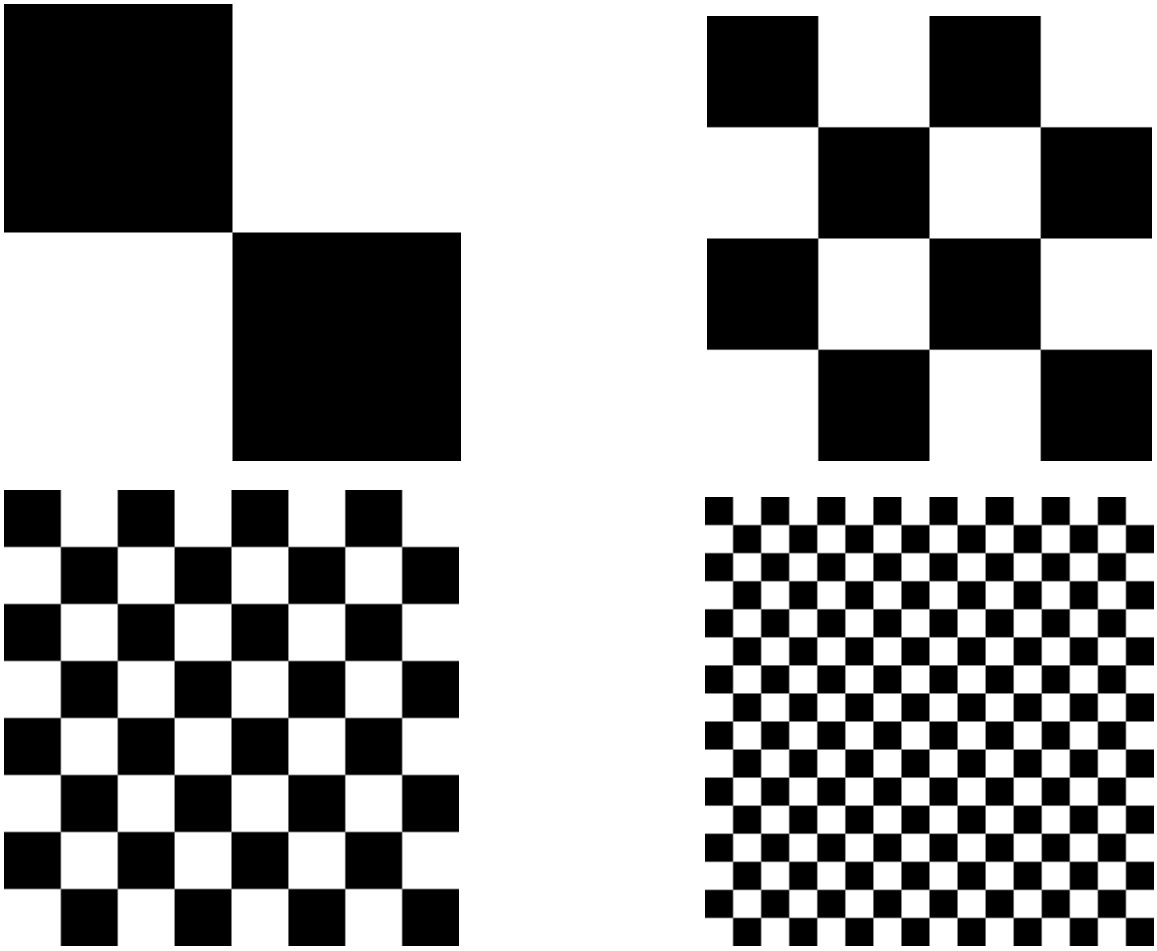

Figure 32. The original images, as drawn using paintbrush. The highest resolution one corresponds to 128 bright spots alternated with 128 dark spots, in each direction. These data were stored repeatedly 48 times in each spot.

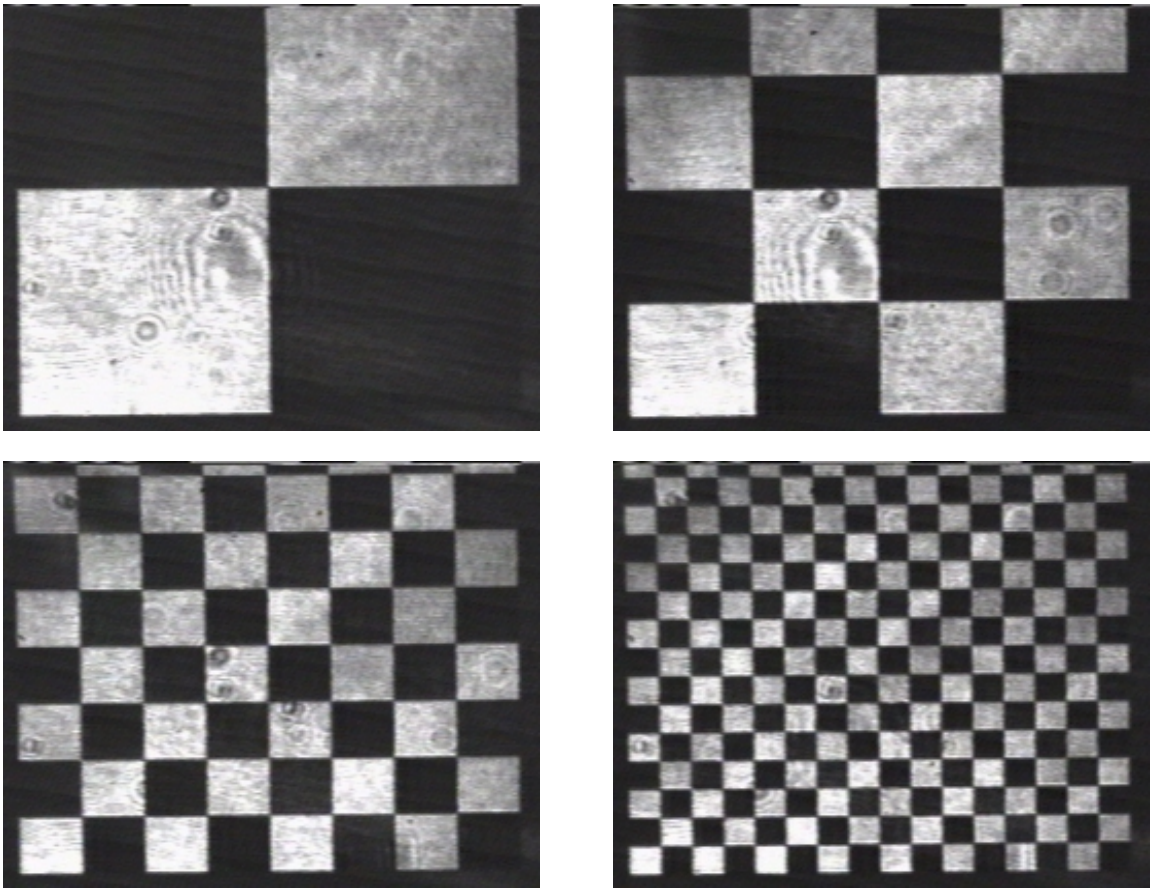

Figure 33. A typical set of reproduced data. The high-resolution images are blurred primarily because of the mismatch between the SLM and the camera pixel elements.

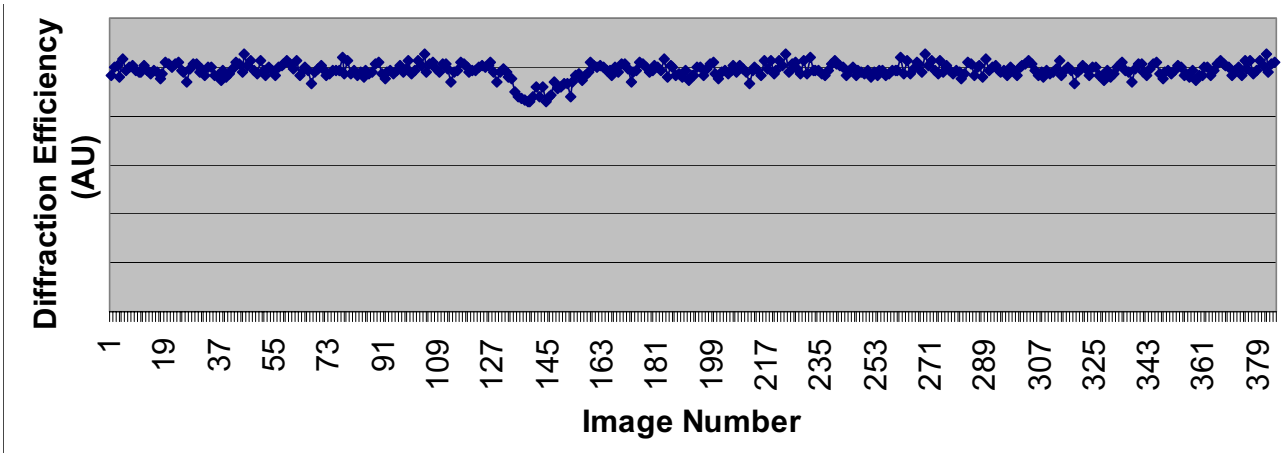

Figure 34. The relative diffraction efficiencies of the 384 data pages at a typical spot. (Ryszard: The little distortion at the start of the second set of 128 is an artifact. We should analyze the data at some other spot to get an even flatter set). No scheduling was used during the writing.